DEVELOPMENT AND TESTING OF A NOVEL MOF-BASED COMPOSITE FOR

MEMS SENSING APPLICATION

by

Bassam Jihad El Taher

A Thesis presented to the Faculty of the
American University of Sharjah
College of Engineering
In Partial Fulfillment
of the Requirements
for the Degree of

Master of Science in
Biomedical Engineering

Sharjah, United Arab Emirates

November 2020

Declaration of Authorship

I declare that this thesis is my own work and, to the best of my knowledge and belief, it does not contain material published or written by a third party, except where permission has been obtained and/or appropriately cited through full and accurate referencing.

Signed: Bassam Jihad El Taher.

Date: 08/11/2020

Approval Signatures

We, the undersigned, approve the Master's Thesis of Bassam Jihad El Taher

Thesis Title: Development and Testing of a Novel MOF-based Composite for MEMS Sensing Applications

Date of Defense: 18/11/2020

Name, Title and Affiliation	Signature
Dr. Mehdi Ghommem Associate Professor, Department of Mechanical Engineering Thesis Advisor	
Dr. Rana Sabouni Associate Professor, Department of Chemical Engineering Thesis Co-Advisor	
Dr. Ghaleb Husseini Professor, Department of Chemical Engineering Thesis Committee Member	
Dr. Paul Nancarrow Associate Professor, Department of Chemical Engineering Thesis Committee Member	
Dr. AbdulRahim Shamayleh Program Coordinator Master of Biomedical Engineering Program	
Dr. Lotfi Romdhane Associate Dean for Graduate Affairs and Research College of Engineering	
Dr. Sirin Tekinay Dean College of Engineering	
Dr. Mohamed El-Tarhuni Vice Provost for Graduate Studies Office of Graduate Studies	

Acknowledgement

Abstract

Mercury is one of the most hazardous environmental pollutants due to its immediate health implications on humans. With the potential of pollution of water due to industrial activities, a need for assessment of mercury levels in waters is needed. Metal organic frameworks (MOFs) have emerged as a new class of crystalline porous materials with potential deployment for chemical detection thanks to their outstanding features. This thesis presents the synthesis of a novel MOF namely NH_2-Cd-BDC that was successfully developed and investigated toward mercury detection in a competitive aqueous medium in presence of other metal ions. NH_2-Cd-BDC is composed of Cadmium ions (Cd^{2+}) as the metal cluster and 2-aminoterephthalic acid (NH_2-H_2BDC) as the organic linker. The luminescent property of the MOF provides a cost-effective and nondestructive method for testing the detection ability of the MOF using fluoro-spectroscopy. The experiments showed that the developed MOF has a limit of detection (LOD) of 0.58 µM and demonstrated the superiority of mercury detection in comparison to other metal ions including Na^+, K^+, Ca^{2+}, Cr^{3+}, Cd^{2+}, Cu^{2+}, Pb^{3+} and Fe^{3+}. Several characterization tests of the novel developed MOF were executed including XRD, FTIR, TGA, FE-SEM and SEM to inspect its crystalline structure and thermal stability. The experimental study revealed that the MOF has a crystalline sea-shell shape, providing a large pore size for the mercury to be trapped in. To investigate how the NH_2-Cd-BDC synthesized stands against other reported MOFs in the literature, three other MOFs, namely NH_2-MIL53(Al), NH_2-MIL88(Fe) and NH_2-UiO-66(Zr), were prepared using microwave-assisted synthesis procedure and their capability to absorb mercury was investigated. All three MOFs comprise the same organic linker (NH_2-H_2BDC) but different metal clusters, Al^{3+}, Zr^{2+} and Fe^{3+}. All the three MOFs are characterized using XRD, FTIR, FE-SEM and TGA. Similar to the novel MOF, the performance of the other three MOFs was assessed by experimenting their capability to detect mercury in presence of aforementioned metals ions. The LOD values were found equal to 0.51 µM, 1.03 µM and 1.94 µM for NH_2-MIL53(Al), NH_2-MIL88(Fe) and NH_2-UiO-66(Zr), respectively. This indicates the suitability of the NH_2-Cd-BDC MOF for mercury sensing applications.

Keywords: *Mercury, detection, metal organic frameworks (MOFs), luminescence property, metal ion selectivity.*

Table of Contents

List of Figures

9

List of Tables

List of Abbreviations

FE-SEM   Field Emission Scanning Electron Microscope

FTIR   Fourier Transform Infrared Spectroscopy

LOD   Limit Of Detection

MEMS   Micro-ElectroMechanical Systems

MOF   Metal Organic Framework

SEM   Scanning Electron Microscope

TGA   Thermal Gravimetric Analysis

XRD   X-Ray Diffraction

Chapter 1. Introduction

1.1.   Overview

Mercury contamination in water bodies across the globe has been rising concerns due to its toxicity for living creatures, bio-accumulative potential and persistence to degradation. Mercury ions get attached to aquatic animals' bodies through chemical bonds formed with protein content that are extremely difficult to break. Upon human consumption of aquatic animals, the mercury content is transferred and magnified to the protein content of the human body. The toxicity of mercury ions then causes major health issues to humans [1], [2].

Metal Organic Frameworks (MOFs) are a new class of composite materials that are gaining high interest in the scientific community. The structures of these MOFs are highly tuneable to suit several engineering applications. MOFs are composed of metal ions (clusters) and organic linkers (organic skeletal compounds with functional groups) attached together to form a material with high porosity. This material can be tailored to have certain chemical and physical characteristics to target specific applications. MOFs have many appealing properties including high porosity and luminescence ability which makes them suitable to detection purposes [3], [4].

In this research, we develop, characterize and analyze MOFs for the detection of mercury in aqueous environments. A novel MOF was synthesized from cadmium and 2-aminoterephathalic acid with the aim to detect low levels of mercury in water. The analysis of the novel MOF includes testing the MOF's ability to detect mercury in a competitive environment, at varying concentrations and inspecting its sensing behavior with other metal ions. Moreover, the performance of the MOF was compared to other promising MOFs reported in the literature for mercury detection. All the MOFs were synthesized using microwave synthesis due to its advantages including providing a fast synthesis route and consuming low energy [5]. Some MOFs weren't reported to have microwave synthesis and this research presented a suitable microwave synthesis route. All MOFs were characterized to gain an insight on their morphology and distinctive structural features.

1.2. Thesis Objectives

Given the serious effects that mercury can cause to humans, this research aims to synthesize a novel material with the capability to effectively detect low mercury levels, in the range of micro-molar, in water bodies. This research utilizes the concept of metal organic frameworks (MOFs) to design a novel derivative of such material that is capable of detecting mercury at low concentrations and in a competitive ionic environment. The objectives of this thesis can be summarized as the following:

- Develop, characterize and test a new MOF that is composed of cadmium ions and 2-aminoterephathalic acid molecules.

- Compare the performance of the novel MOF to previously reported MOFs in literature. The comparison is to be made by synthesizing three competitor MOFs in-house. All the MOFs are to be characterized and tested for detection performance.

1.3. Research Contribution

The contributions of this research work can be summarized as follows:

- Synthesis, characterization and analysis of a novel MOF, namely NH_2-Cd-BDC, made of cadmium metal ions and 2-aminotelephathlic acid molecules using microwave-assisted heating. The MOF was capable of detecting low concentrations of mercury and showed excellent performance in presence with other metal ions in the aqueous environment at higher concentration.

- Synthesis of similar MOFs composing the same organic linker and three different metal ions, Al^{3+}, Zr^{3+} and Fe^{3+}. All MOFs were prepared using microwave-assisted synthesis, which provided new synthesis route for some of these MOFs.

- Comparative performance analysis of the four aforementioned MOFs. The comparative analysis aimed at understanding the performance level of the novel MOF compared to previously reported MOFs.

1.4. Thesis Organization

The rest of the thesis is organized as follows: Chapter 2 provides a detailed background and literature review about mercury, MOFs and microwave-assisted synthesis for MOFs. The synthesis procedure, characterization and testing of the novel

MOF are discussed in Chapter 3. Chapter 4 presents the comparative analysis of four different MOFs developed in this research. Finally, Chapter 5 concludes the thesis and outlines the future work.

Chapter 2. Literature Review

2.1. Mercury

Heavy metals contamination in water bodies have been raising concerns across the scientific community due to their high toxicity. Heavy metals are a group used to describe some of the transition metals found in the periodic table. Arsenic, lead, chromium and mercury are some of the heavy metals that have serious impact on humans and aquaculture animals [6]. These environmental pollutants are usually released into open water via several sources including coal-burning electric utilities, chlorine and cement manufacturing plants, battery wastage and spills from electronics spares [7]–[9]. The entry point of heavy metals to water sources are numerous and include dissociation of metal salts deposited as waste from industries [10], landfill leachate that could reach nearby water sources and it might contain heavy metal ions in it [11]. Also, air pollution that can carry these metal ions in gaseous forms, where they can dissolve in the water upon direct contact [12]. Hence, it is very difficult to control water pollution and it sources.

Mercury (Hg) is one of the most hazardous environmental pollutants due to the bioaccumulation of the ions in the body of recipients. Mercury ions have a special property that allows them to have a high affinity to the amide group (NH_2), which is found readily in the human body as it present in lipids and proteins. This high affinity results in the mercury forming a bond with the proteins that makes it extremely hard for the human system to remove [13]. Hence, the phenomena of bioaccumulation results in mercury concentration increasing in the human body over the years. This mercury bonding causes major health problems for humans such as kidney failure, damage of the neurological systems and can eventually lead to fatality when the concentration exceeds 0.00003 mg/L [1]. Also, a concept of bio-magnification occurs as the mercury concentration gets intensified with the fishes and aquatic animals feeding upon each other [14].

Mercury entry point to the water is usually through the gas known as methylmercury (MeHg). This gas can be released naturally due to volcanic eruptions or can be released industrially due to the degasification process during mining [15]. The released methylmercury is soluble in water and infiltrates it to bind to aquatic animal and/or plants. The binding happens as the mercury ion breaks apparat from the

methylmercury ion complex and becomes free to bind. As stated above, the natural tendency of the mercury ion allows it to easily bind to the plants and/or animals as they are rich in lipids containing NH_2 functional groups [16]. According to the studies reported in the recent paper by Yang et al. [17], the amount of mercury present in waters has gone up by 10-12 times ever since the beginning of the industrial revolution. Due to the growing concern for higher mercury concentrations in aquacultures and the aforementioned consequences on human health, there is an urgent need to assess the contamination of coastal sea water on a regular basis to ensure safe and sustainable fishery products [17].

2.2. Current Detection Methods of Mercury

Currently some detection methods of mercury exist. First type of detection is batch sampling, where water samples are withdrawn and sent to laboratories. These laboratories use either Chromatography or atomic spectroscopy to quantify the mercury level in the samples [18]. These techniques are highly accurate but they are expensive, due to the high capital cost of the equipment. Additionally, the batch nature of the detection method provides a disadvantage and presents an opportunity for the development of a more independent and real time system. Moreover, another common method for detection of Mercury is using a cell microbial sensor. This basically utilizes the DNA of cells that allows to bind to Mercury ions and compound forms of Mercury. The result of this binding is causing a change to the cell structure due to the capture of mercury [19]. The disadvantage of this technique is the complexity of quantifying the detection amount of Mercury and the sophisticated maintenance required to ensure the cells are not dis-functionalized. Thus, an alternative chemical sensor is needed that allows for an inexpensive set-up and can operate in a robust environment.

In addition to the specified methods above, scientists and researchers have continued on developing new materials to detect mercury in aqueous solutions. The materials synthesized were adopting the new insights gained about chemical compounds and their properties to produce materials with desired characteristics. In particular, the characteristics of such materials, need to ensure high selectivity to mercury in a competitive water environment of different ions, high water stability and most importantly a low limit of detection that allows for capturing very small concentrations of mercury as required in several engineering applications [20]. For

instance, Prakashan et al. [21] developed a copper-silver core shell nanoparticles coated with SiO_2-TiO_2-ZrO_2 ternary matrix to detect mercury. The SE nanoparticles were tested for mercury detection in aqueous solutions and the material limit of detection was found equal to 0.01 µM. The material was also tested with other ions and was proven to have high selectivity for mercury [21]. These materials provide a solid basis for understanding the mercury detection mechanism. However, the deployment of such materials requires sophisticated and costly equipment. Wu et al. [22] synthesized a coumarin probe that has the ability to detect mercury in aqueous solutions. Coumarin is a metal organic compound that belongs to the class of aromatic organic compounds. The coumarin is joined with a chemical additive and is capable of detecting mercury at low concentrations, where the LOD was reported to be 0.12 µM. The coumarin probe also possess a fluorescence property that enables it to be easily used for detecting mercury without the need for any expensive equipment. However, the coumarin probe shows no regeneration capibilities, meaning that the bond formed between the coumarin and mercury is so strong that it cannot be broken. Hence, the coumarin probe can be only used one time and then needs to be disposed [22].

2.3. Metal Organic Frameworks (MOFs)

In order to assess the mercury threat in water bodies, the deployment of chemical sensors with the capability to conduct real-time and in-situ measurements is needed. The development and analysis of chemical sensors for the detection of different ions and environmental pollutants have been the topic of several research studies [23]–[25]. These chemical sensors have advanced to be at the Nano-scale to prevent disruptions in the water ecology [23]. Nanomaterials are used in many applications such as in drug delivery applications [24], chemical sensing [25] and separation and filtration purposes [26]. A special and highly capable class of material that can be prepared at the Nano-scale is Metal Organic Frameworks (MOFs). MOFs are a new class of crystalline porous material with potential in several engineering applications. MOFs have gained significant interest as promising material thanks to their outstanding characteristics that include ease of modification and functionalization to selectively detect a specific chemical, tunable pore size and luminescence [27], [28]. These properties have allowed MOFs to be successfully deployed in a wide range of engineering applications such as; gas separation [29], heterogeneous catalysis [30], removal of micro pollutants [31], [32], pharmaceutical manufacturing processes [33] drug delivery carriers [34], [35] and

17

chemical sensing [29]. MOFs are composed of a metal cluster that hold organic linkers together in a rather stable structure. The metal cluster is a simple metal ion (or can be a complex ionic structure of different ions) and the organic linker is an organic skeleton with different active groups attached to it [31]. Surface modifications and functionalizing of MOFs play a vital role in designing high performance materials for targeting specific analytes (e.g. Hg^{2+}) for simultaneous sensing and removal. In addition, porosity is an important property that is studied extensively to analyze the ability of the MOF in the removal of analytes. All MOFs are known to be porous but have different voids according to the MOF's structure and constituents used. The porosity of the MOF is usually examined using a Brunauer-Emmett-Teller (BET) test. The BET test gives numerical measurement of the voids and the MOFs adsorption capacity, which is helpful in the case of removal scenarios [36]. Also MOFs possess a very important property that allows them to be used for the sensing applications, which is the regeneration ability. Upon detecting the material through chemical or physical bonding, a reagent can be used to undo the bonding reaction. This is known as regeneration and it allows the same MOF to be used several times before it becomes ineffective. This is considered an exceptional property that allows for industrial use as it is a cost-saving material [37]–[40]. MOFs have recently started being produced in large quantities by large chemical manufacturers, such as Sigma Aldrich. However, many are still only found in literature in journal databases due to the high tune-ability of the material. For example, Ruiz et al. synthesized a tuned version of the commercially sold ZIF-8 MOF. The ZIF-8 MOF is commercially sold but the researchers self-assembly it on to a beam to allow for the detection of CO_2 gas. The produced sensor showed high capability of CO_2 detection and presented a potential sensor assembly that can be utilized for further sensing applications in the near future [41].

  2.3.1. Microwave-assisted synthesis for MOFs. An important advantage of MOF is the ease of synthesis, where a solution is usually prepared and then heated to allow for the formation of the rigid structure. To date, most commonly heating mechanisms used for the preparation of MOFs are based on conventional-solvothermal methods, which require long synthesis time and high energy consumption [42]. As a result, the development of new alternative methods has been attracting a great interest among researchers and scientists including: microwave irradiation [43], sonochemical

irradiation [44], mechanochemical [45] and ultrasonic methods [46]. The present research work focuses on the use of microwave irradiation as a synthesis technique rather than the conventional solvothermal method due to several advantages. Indeed, microwave irradiation uses the known microwave frequency wavelengths to create a heating effect using either dipole rotation or ionic conduction [47]. This heating mechanism provides more intensive power per unit time when compared to the regular solvothermal heating, which constitutes the basic mechanism of conventional laboratory ovens. This greatly shortens the time needed for the reaction to happen from several days to few minutes. This constitutes one of the major advantages of using microwave irradiation [47], [48]. Furthermore, microwave irradiation does not affect the morphology of the material to be produced. For example, the produced material would preserve its crystalline structure when using microwave irradiation [5]. Another advantage that make the synthesis of MOFs using microwave more favorable over the conventional oven is its low energy consumption levels [47]. As such, several research groups have successfully used microwave irradiation for the synthesis of MOFs [49].

      2.3.2. Amino-functionalized MOFs. Recently amino-functionalized MOFs have attracted a noticeable attention mainly due to their high fluorescence ability [39], [50] and for their Hg^{2+} detection, given the strong coordination between the amino group and Hg^{2+} ions [50], [51]. The NH_2 group present in amino acids provides a strong linkage point which attracts the mercury ions and allows for the formation of a complex ion. This attraction to the NH_2 group is caused due to the NH_2 being a nucleophilic center. Nucleophilic centers are molecules with a tendency of pairing due to their ability to share electrons. The partial polarization concept offer occurs in these nucleophilic centers due to the difference in electronegativity. Mercury, being a positively charged ion, gets attached firmly to the nucleophilic center as the positive charge gets attracted to the free electrons the nucleophile is giving [52]. This complex ion formation, resulting from a substitution reaction, ensures bonding of the mercury ion. This formation leads to a change in the structure of the amino group and then affects the MOF fluorescence and weight. This feature allows for cost-effective and simple detection mechanism using fluoro-spectrocopy [50], [51]. Moreover, this allows for a higher selectivity towards mercury ions as well in a competitive environment [52]. Figure 1 below shows how the mercury attachment happens, which is based on a

Zirconium MOF published in literature that can detect mercury due to the functionalized amino group.
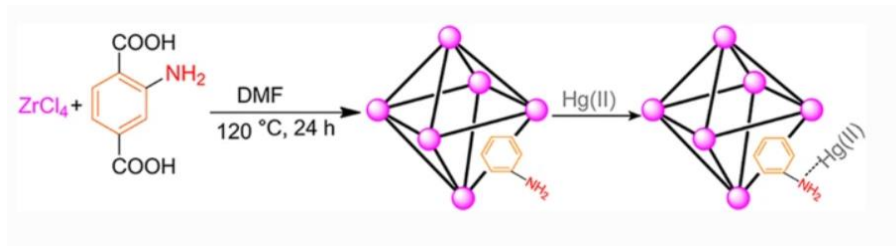
Figure 1: Amino-functionalized MOF synthesis and mercury attachment to amino-functional group [53].

An example of MOFs synthesized using amino-functionalized MOFs is the MOF synthesized by Zhang et al. [54] which contained an amino-functionalized organic linker. The organic linker had the standard carbon-hydrogen backbone but was modified by adding several functionalization groups. These functionalization groups aimed at providing mercury with more active sites for binding and allowed for structure maintenance after mercury adsorption. The metal cluster used for the MOF was copper and the MOF was synthesized using the regular solvo-thermal method. The MOF was tested against other metal ions and showed very little or no response to them. The limit of detection of the MOF was determined to be 5.88 µM. In addition, Xia et al. [55] synthesized different MOFs using the same metal cluster but different organic linkers. The purpose of the study to see how the different organic linkers that have different amount of amino-functionalized groups could affect the mercury detection ability of the MOF. Amongst the organic linkers, T_bTATAB was found out to have the best detection abilities towards mercury. This is due to the pore size and accessibility of that the mercury enjoys in the structure of T_bTATAB. This allows the MOF to be quite effective in capturing mercury ions. The limit of detection of the material was determined to be 4.4 nM, showing the great abilities the MOF can have in detecting mercury at very low concentrations. Many examples from literature use amino-functionalized MOFs to prepare sensors that are capable of adsorbing mercury in aqueous solutions. Some of these MOFs are mentioned below in the proceeding section.

2.3.3. Luminescent MOFs for mercury from literature. MOFs have numerous advantages for use as detector material including their luminescence ability,

high surface area, short response time, high removal efficiency and tailor-ability of the surface functionality. These MOFs have been extensively investigated for mercury adsorption and have caught interest due to the ease in the detection mechanism. Luminescent MOFs are materials that possess the property of glowing under certain wavelength of the electromagnetic spectrum. The wavelength of light emission depends on the compounds constituting the MOF, where different organic linkers and metal ions have different wavelengths that excite their electrons. It allows then for the use of relatively inexpensive detection method such as the fluoro-spectrometer to inspect the detection capability of the MOF [31], [32]. Wu et al. [33] developed Cd-EDDA luminescent MOF for mercury detection in aqueous solutions. The produced MOF has shown an instantaneous response and high selectivity for mercury ions in aqueous media. The use of cadmium ions in the metal cluster adds to the luminescence property of the MOF. The limit of detection of the MOF was measured and found equal to at 2 nM [33].

Yang et al. [34] synthesized and tested two cadmium based MOFs that had the potential of detecting heavy metals inside water. The first cadmium-based MOF was developed using $Cd(OAc)_2 \cdot 2H_2O$ and NH_2-H_2BDC producing a MOF that has a long chain of OAc and the NH2-H2BDC attached to cadmium. This MOF was tested for the detection ability and was found to have a very high selectivity for copper ions with a LOD of 1.2 µM. The second MOF developed was also containing cadmium as its metal cluster but had a different organic linker known as H_2tbta. This organic linker contains bromine ions attached to an organic skeleton similar to the one found in the NH_2-H_2BDC. This MOF was observed to be selective for mercury ions in aqueous solutions with a LOD of 0.29 µM [34]. Su et al. [56] synthesized a new MOF that is composed of cobalt (Co (II)) as the metal cluster and 4,4′-(hexafluoroisopropylidene)diphthalic acid) (4,4′-bis(imidazol-1-yl)-biphenyl, H4hfpd) as the organic linker. This MOF was tested for mercury detection and showed great ability to immediately detect mercury in a competitive environment in presence of several heavy metal ions. The performance of the MOF was assessed for low concentrations of mercury. It showed a limit of detection of 4 µM. This value was obtained by examining the fluorescence quenching when the Co(II)-based MOF is exposed to mercury ions at different concentrations [56].

21

Sun et al. [57] used the commercially produced MOFs for mercury detecting. Fe-BTC is a commercially sold MOF that can be found at chemical stores retailers. The researchers modified the MOF structure by treating it with dopamine and a spontaneous reaction causes the dopamine to polymerize and form polydopamine. Hence, the new synthesized MOF is known as Fe-BTC/PDA. The new MOF exhibited high detection properties for mercury ions as well as lead ions. The experiments revealed that the MOF can uptake up to 394 mg of Pb^{3+} and 1634 mg of Hg^{2+} per gram of the MOF. The MOF was tested on a 1 ppm solution and showed a removal rate of 99.8% of the ions [57]. Liu et al. [51] prepared a MOF known as Cd-H_3TATAB that composes of Cadmium as the metal cluster and 4,4′,4″-s-triazin- 1,3,5-triyltri-p-aminobenzoic acid (H_3TATAB) as the organic linker. Moreover, the MOF was tested for Mercury detection and proven the ability to detect Mercury in a competitive environment in a rapidly fashion. The MOF was tested on a concentration of 1 mM and proven its detection abilities by observing how the fluorescence quenched when the Cd-H_3TATAB captured the Mercury ions. However, the limit of detection was not reported in this study. The Cd-H_3TATAB has a fluorescence emission at around 360-365 nm at an excitation of 310 nm. Also, the study included the behaviour of the Cd-H_3TATAB at different concentrations of Mercury. However, the synthesis of the Cd-H_3TATAB was done using the traditional laboratory oven and it takes 72 hours (3 days) continuously being heated in the oven. According to Liu et al., the physical properties of the Cd-H_3TATAB is that it is a solid yellow powder at room temperature [51]. Furthermore, the Cd-H_3TATAB MOF has a tetragonal shape as presented in Figure 2.
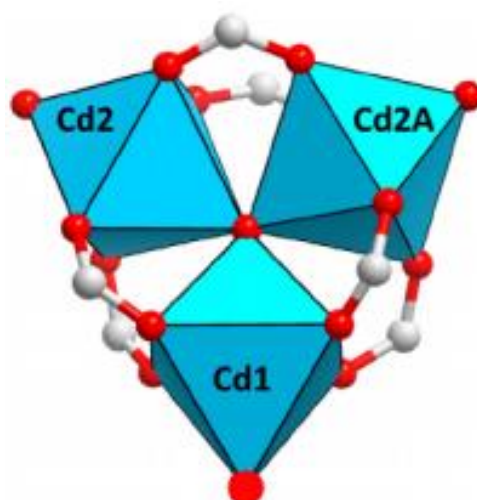
Figure 2: 3D image of the structure of the Cd-H3TATAB MOF [59].
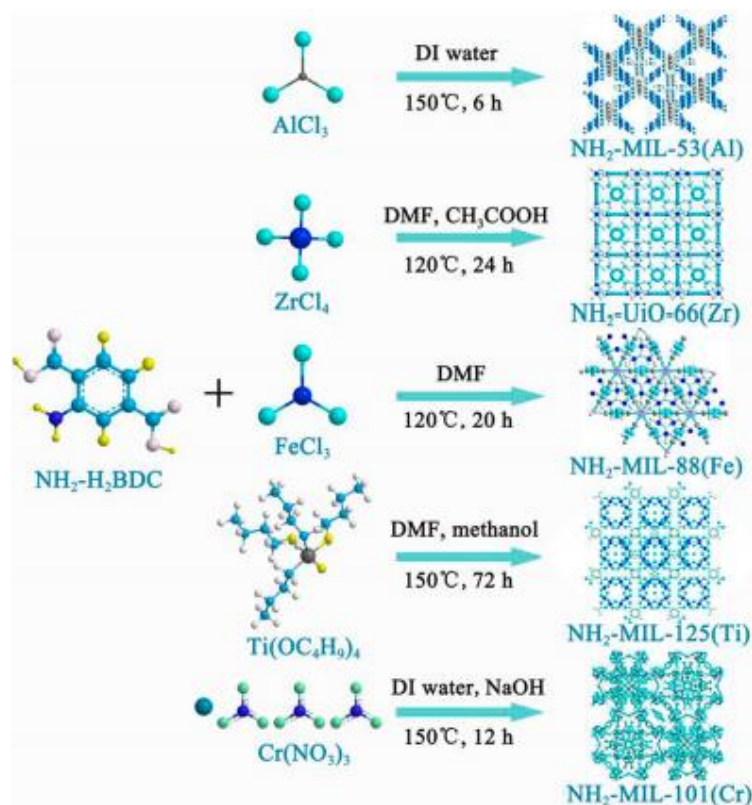
Figure 3: The different MOFs produced by Zhang et al. [58] and the synthesis routes of each MOF [58].

Xie et al. [58] synthesized a Fe-MOF for mercury detection purposes. The NH_2-MIL88 (Fe) MOF synthesized is composed of Fe^{3+} as the metal cluster and the NH_2-H_2BDC as the organic linker. However, the MOF was synthesized with the aim to reduce the size of the particles for better water deployment. The MOF was synthesized using the regular solvo-thermal synthesis at 120°C for 20 hours. The Fe-MOF exhibited performance in mercury detection as anticipated and was capable of detecting mercury at low concentrations, up to 40 ppb [58]. Zhang et al. [50] developed five MOFs combining the organic linker NH_2-H_2BDC with different metal clusters (Al^{3+}, Fe^{3+}, Ti^{4+}, Zr^{4+} and Cr^{3+}) and investigated their detection capability of mercury. Their experimental study revealed that the MOFs made of aluminum and iron ions have the highest detection abilities. The aluminum based MOF showed the most superior detection performance. The developed MOFs have fluorescence abilities that facilitate the inspection of their detection capability using the fluoro-spectroscopy meter. The excitation level of the MOFs were all set at a wavelength of 330 nm and the emission was detected around 427 nm. The authors performed a detailed analysis of the MOFs

23

detection abilities by quantifying the limit of detection (LOD). To do so, they investigated the detection at various levels of mercury and in a competitive environment with other metal ions. The reported LOD was 0.15 µM for the aluminum based MOF which was identified as the best candidate for mercury detection. The study also featured a pH analysis to show how the MOF detection varied with different pH values. Furthermore, the Al-MOF's absorption capabilities was investigated in the study too and reported promising absorption behavior and capabilities of the MOF. The synthesis routes are summarized in Figure 3 [50].

2.4.   MEMS

The recent advances in micromachining technology has boosted the development of miniaturized gas and chemical sensors at reduced manufacturing cost and time with improved performance, high reliability, easy integration with electronic circuits and low power consumption. In particular, the deployment of electrically-actuated vibrating micro-beams for gas and chemical sensing has gained significant interest in the last few years thanks to their outstanding dynamic features in response to small variations in their effective mass (on the order of femto- to picogram) and when vibrating in different fluid domains. The microbeams are usually coated with a sorbent layer (eg. polymer) with an affinity to the gas or chemical of interest to be detected [59]. Wang et al. [60], has developed a gas sensing device that can detect various gaseous compounds such as ammonia and ethyl glycol with concentration as low as 1 ppm. The researchers developed the microsystem with a total area of 3 mm^2 and used CMOS integrated system for developing the sensor signal reader. The mechanism of gas sensing is simple, where the cantilever is hinged on a fixed surface from one side and when the gas comes in contact with it, the material on the cantilever captures the gaseous compounds (similar to what MOFs do), this capturing causes a change in the weight of the cantilever and causes it to bend and vibrate more vigorously. As a result of this, the electrical system captures this vibration and translates it to a concentration based on the amplitude and frequency of the vibrations. A calibration curve that is already designed will be used to do the conversion. Many factors such as natural frequency of vibration, MOF detection abilities and the air dynamics are all factors that the system to be designed to account for to provide the accurate reading [60]. Prajesh and Khanna have utilized the micro-cantilever technology to develop a gas sensing to detect Ammonia. The researchers were able to develop the system to withstand

temperatures as high as 250 °C and all need 68mW. Again, the advantages of the micro-beams and MEMs system is the small size it has, as this one was developed to have a size of 30 micrometer [61]. Moreover, researchers have started investigating the ability to develop such systems for liquids; however, the liquids MEMs systems are way more complicated due to the fact that the parameters controlling the motion (in the gas phase, it was the air dynamics) are now more complicated because of the introduction of the water motion. In the gas sensing application, the cantilever was hinged to one side and that reduce the level of noise the system experiences, but in the case of the liquid, movements of the liquid can cause distortion of the values. Moreover, if it was water and the case of aquatic farms as in the case of this research, the tidal waves and fishes interaction can cause large noises in the frequency curves and may cause faulty readings; thus, all these values needed to be taken into account [60].

2.4.1. Integration of MOF with MEMS technology. Combination of the concept of MOFs and MEMS technology can be used to produce an effective chemical sensor that can detect various chemicals. These MEMS chemical sensors able effective, real-time and highly sensitive detection to a target analyte. These sensors are usually composed of the silicon micro-beams coated with MOF and some electrical components to convert a small change in the effective mass resulting from the deposition of the target analyte on the micro-beam into a resolvable signal [62]. To secure an effective detection, the MOF needs to be properly adhered to the silicon micro-beam [63]. Several observations can be made on the adhering material to be selected for the purpose of depositing the MOF on the silicon-micro-beam. First, the MOF needs to stick firmly to the micro-beam surface, so the adhering material needs to have a high water resistance. Second, the adhering material needs to not interfere with the MOF and its chemical properties [64]. Hence, upon literature investigation, polyimide Matrimid was found to be one of the suitable adhering materials to cause the MOF attach firmly on to the micro-beam [65]. The research work by Koper et al. [65] showed that the polymer caused great adhering abilities and proved successful in gas sensing applications. Given that the gas environment is vigorous than the water environment, the polyimide needs to be further tested for its capabilities of withstanding the water environment. Koper et al. [65] proposed an facile deposition method of the MOF on to the micro-beam using a micro-dropper. The technique uses a solvent that dissolves the polyimide Matrimid and the MOF together. The solvent used in this work

was ethanol due to its high volatility. Then the solution is deposited on the micro-beam using a micro-dropper. The used solvent is observed to have a high volatility such that it evaporates immediately upon deposition [65].

Chapter 3. Synthesis, Characterization and Performance Analysis of NH2-Cd-BDC MOF

In this chapter[1], the novel luminescent MOF synthesized for mercury detection in aqueous media via facile microwave irradiation method is presented. The synthesized MOF is composed of the metal cluster of cadmium (Cd^{2+}) and the luminescent organic linker NH_2-H_2BDC. A series of experiments is conducted to investigate the ability of the proposed MOF to detect mercury in water, determine its LOD and demonstrate its superior performance in a competitive environment in presence of other heavy metal ions. The experimental study investigates the structure of this newly developed MOF by performing characterization tests including XRD, FTIR, FE-SEM, SEM and TGA

3.1. Materials and Methods

3.1.1. Materials. All the chemicals used in the present study were purchased from Sigma Aldrich through its local supplier in the UAE, LabCo. These chemicals are cadmium (II) perchlorate hexahydrate: $Cd(ClO_4)_2 \bullet 6H_2O$, 2-aminoterephthalic acid: NH_2-H_2BDC, Dimethylformamide (DMF): C_3H_7NO, methanol: CH_3OH, Hydrochloric acid: HCl and Mercury (II) nitrate monohydrate: $Hg(NO_3)_2 \bullet H_2O$. All chemicals had a reported purity of 99% from the supplier. All materials were used without further modification except for the hydrochloric acid (HCl) which was diluted to match the required concentration of 2 M from its original concentration of 10 M.

The synthesis of the MOF was carried out using the laboratory microwave oven (MDS-6G Digestion, Sineo). The laboratory microwave can take up to 8 reaction vessels at one time and allows to input heating loads as step wise functions [66]. The fluorescence measurements were carried out using the QuantaMaster 300 Phosphorescence Spectrometer from PTI, (Horiba LTD, Kyoto Japan) [67]. The equipment is accompanied with the software FelixGX Version 4.0.1., used to capture, record and process the readings of the spectrofluorometer [68]. The sample drying was done using the standard laboratory oven of mode FD-23 from Binder (Binder, New York USA) [69].

3.1.2. Characterization. The Fourier Transform Infrared (FTIR) spectra were recorded from a PerkinElmer spectrophotometer, USA in pressed-disc technique using KBr pellets. The operating range of the FTIR was set from 4000 to 500 cm-1, with 10 scans being signal-averaged having a resolution of 1.0 cm^{-1} [70]. The X-Ray Diffraction (XRD) pattern were performed using D8 ADVANCE system from Bruker [71]. The XRD was set at a 2θ range from $5.0°$ to $50.0°$. The step size was $0.03°$. The surface morphology measurements were recorded with TESCAN, model VEGA3 Emission Scanning Electron Microscope (SEM) [72]. The SEM was carried using two magnifications, 10 µm and 5 µm voltages of 10.0 kV for HV and 5.00 kV for MAG. The Field Emission Scanning Electron Microscope (FE-SEM) was recorded using Apreo C FE-SEM model from ThermoFisher Scientific, Czech Republic [73]. The FE-SEM was carried using two magnifications, 1 µm and 500 nm voltages of 5.00 kV for HV. The thermogravimetric analysis (TGA) of dry NH_2-Cd-BDC sample was performed using the thermogravimetric analyzer from Shimadzu, Japan [74]. The TGA analyses were performed 30°C to 800°C at a heating rate of 10°C/min under air. All characterization results were plotted using Matlab. The Dynamic Light Scattering (DLS) for the particle size measurements were recorded using DynaPro NanoStar from Wyatt technology. The DLS settings were pre-built in for recording measurements.
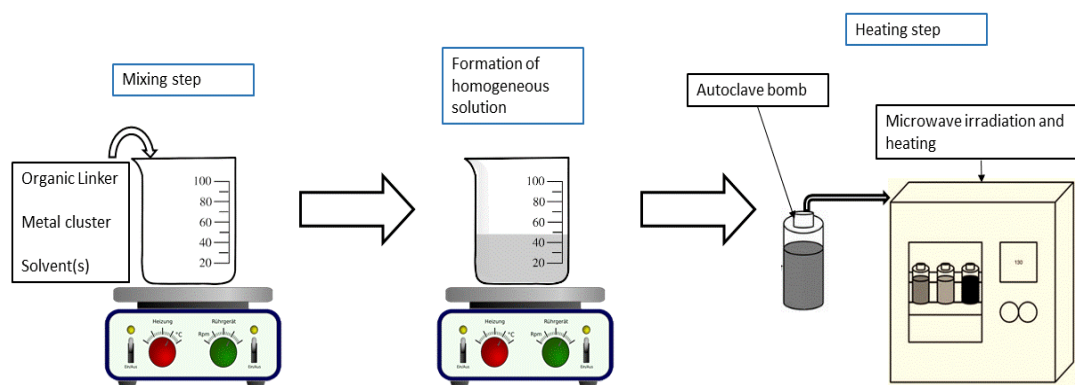
Figure 4: Experimental procedure for the synthesis of the MOF. The steps include addition of the chemicals, formation of the homogenous solution and heating of the solution to form the MOFs using microwave-oven.

3.1.3. Synthesis of NH2-Cd-BDC. Figure 4 illustrates the main experimental steps carried out for the synthesis procedure. The proposed MOF was synthesized by dissolving 0.251 gram of NH_2-H_2BDC in 20 mL of DMF. Then, 0.580 gram of cadmium (II) perchlorate Hexahydrate $Cd(ClO_4)_2 \cdot 6H_2O$ was added to the solution with

28

2 mL of methanol and 0.4 mL of 2M HCl. The obtained mixture solution was transferred into a 50 mL Teflon-lined microwave reaction vessel and heated at 120℃ for 75 minutes at 800 W. The obtained brownish powder was collected by centrifugation for 3 minutes at 4000 rpm and washed three times with DMF. Finally, the collected MOFs were dried in oven at 80°C for 1 hour and labeled as NH_2-Cd-BDC.

3.1.4. Testing NH2-Cd-BDC. The testing procedures for the NH_2-Cd-BDC MOF will be explained in this section.

3.1.4.1 Single metal ion detection. To test the photo-luminescent (PL) performance of the developed MOF, a stock aqueous solution of 1.3 mg NH_2-Cd-BDC and 250 mL of deionized water (baseline solution) was prepared. The aqueous solution was sonicated for 10 minutes to obtain the homogeneous suspension. The fluorescence of the baseline exhibited an intense emission band at 427nm upon excitation at 330 nm as shown in Figure 11. Separate solutions were prepared for 9 different ions, these ions are: Hg^{2+}, Na^+, K^+, Ca^{2+}, Cr^{3+}, Cd^{2+}, Cu^{2+}, $Pb^{3+}$and Fe^{3+}. The metal salts used to generate these metal ions are mercury (II) nitrate, sodium chloride, potassium chloride, calcium chloride, chromium (III) nitrate, cadmium (II) perchlorate, copper (II) sulfate, lead (II) nitrate and iron (III) chloride, respectively. These metal salts were selectively chosen due to their solubility in water. All prepared solutions had a fixed concentration of 1000 µM. Next, the luminescent response of the NH_2-Cd-BDC suspension was tested. This was executed by taking 2 mL of the MOF suspension and adding 0.5 mL of the ions solutions separately. This gave a final solution with a concentration of 200 µM of the different ions. The final solution luminescence was tested and probed at the same excitation band of 330nm as shown in Figure 13 and Figure 14. The readings for fluorescence were taken by the QuantaMaster 300 Phosphorescence and fluorescence spectrometer as discussed in the Materials and Methods section. The excitation was set at 330 nm and the range for emission is set between 350 nm and 600 nm. Also, the PMT detector voltage was fixed at 726 V.

The quenching efficiency of the MOF due to ion adsorption, which constitutes the main performance metric in our analysis, was reported as a percentage. This percentage is calculated based on the difference between the fluorescence intensity of the initial MOF with water without the analyte ($I_{baseline}$) and the fluorescence intensity of the MOF with the presence of an analyte ($I_{immediate}$) as expressed in Equation (1):

$$\frac{I}{I_o}\% = \frac{I_{immediate}}{I_{baseline}} * 100 \qquad (1)$$

3.1.4.2 Limit of detection (LOD). In addition to the quenching efficiency, the Stern-Volmer (SV) equation was used to further evaluate the quenching effect [50]. This equation is given by:

$$\frac{I_o}{I} = 1 + K_{SV}[M] \qquad (2)$$

where *I* (a.u) and I_o (a.u) represents the fluorescence intensity of the MOFs in the presence and absence of the analyte, respectively. The K_{SV} (M^{-1}) represents the Stern-Volmer constant and the [*M*] (M) represents the molar concentration of the target. Furthermore, the limit of detection (LOD) experiment was conducted similar to that of the single ion as mentioned above, where 0.5 mL of different concentration of Hg^{2+} solution (5 µM – 1000 µM) was added to 2 mL of the MOF stock solution so that the final concentration range is 1 µM – 200 µM. Based on the Stern-Volmer (SV) equation, the LOD was determined by testing the mercury quenching at different concentrations (200 µM to 1 µM). Figure 15 illustrates the quenching of the MOF when exposed to mercury of different concentrations. The LOD was calculated based on the following equation [50]:

$$LOD = \frac{3 * SD}{m} \qquad (3)$$

where *SD* represents the standard deviation of the error (standard error of regression) and *m* is the slope of the best fit for the low concentrations curve presented in Figure 16. The values reported in the y-axis were obtained by computing (*I/I_o* – *1*), where *I* and I_o denote the fluorescence intensity in the presence and absence of the analyte, respectively. The graph shown in Figure 16 is based on the computation of the Stern-Volmer equation [50]. To verify the repeatability of the experiments, 6 replicates were considered to identify the LOD of the developed MOF. The average of the intensity measurements was computed to calculate the value of (*I/I_o* – *1*). The obtained value of LOD is based on the average of these 6 trials and the error bars are reported in Figure

16 to confirm the consistency of the experimental measurements, despite the low mercury concentration considered in the LOD experiments. Similarly, the LOD of the developed MOF for Iron was computed using 3 experiments replicates and following the same calculation procedure. The obtained LOD for Iron is reported along with the Stern-Volmer graphical representation as shown in Figure 18 which also contains the error bars indicating a slight deviation in the experimental results.

3.1.4.3 Competition and selectivity. Given the complexity of the detection mechanism in real water matrix, the detection selectivity of NH_2-Cd-BDC constitutes an important factor that should be investigated to ensure the operability of the MOF for real scenarios. To assess the capability of NH_2-Cd-BDC to act as a highly selective probe for Hg^{2+} in the presence of other competing metal ions, suspensions of MOFs containing Hg^{2+} were spiked with various metal ions including: Na^+, K^+, Ca^{2+}, Cr^{3+}, Cd^{2+}, Cu^{2+}, Pb^{3+} and Fe^{3+}, while doubling their concentration with respect to that of mercury. Then, the fluorescence change in the photoluminescence of the mixture was measured. Figure 19 shows the results of the conducted competition test.

We note that all experimental results were processed and plotted using the software tool Matlab.

3.2. Results and Discussion

3.2.1. Characterization. In order to develop a good understanding of the structure of the newly developed MOF (NH_2-Cd-BDC) and its detection mechanism, several characterization tests were conducted including: XRD, FTIR, FE-SEM, TGA and SEM. The XRD test was performed on three samples: a fresh sample, a sample kept overnight in water and a sample after Hg^{2+} ions detection/adsorption. The results are displayed in Figure 5. The fresh sample result provides an insight on the crystal structure of the developed MOF (Figure 5(a)). We observe the occurrence of peaks approximately at 13°, 19° and 27°, which are unique for the newly-produced MOF. These sharp peaks indicates that the MOF has a solid crystalline structure, rather than being an amorphous structured MOF. Water stability of the MOF was also studied by taking into consideration the fact that the MOF will be deployed in water to detect Hg^{2+} ions. A sample of MOF was soaked in water overnight and then the XRD test was conducted to inspect any possible change in the structure due to the exposure to water. The corresponding XRD results are shown in Figure 5(b). An overall overlap was

clearly observed between the two patterns. This indicates that the MOF NH_2-Cd-BDC maintained its crystalline structure and did not experience any potential collapse after being soaked in water for a period of time. The intensity of some peaks have been reduced in comparison to their counterparts in Figure 5(a). Yet, they still maintained their sharpness and did not convert to wider peaks. This confirms that the structure remained crystalline. Moreover, Figure 5(c) presents the XRD of the NH_2-Cd-BDC after detection of mercury ions. Upon comparison with the XRD of the fresh sample, we observed some difference in the intensity of some peaks of Figure 5(a) and Figure 5(c). For example, the intensity of the peaks at 10° and 20° is much higher in Figure 5(c) compared to Figure 5(a). Moreover, a few peaks appear in the XRD pattern besides the pattern of NH_2-Cd-BDC. For example, the new peak observed at around 7° and 22º in Figure 5(c). The third observation is the noticeable decrease in the degree of crystallinity of the MOF. This can be observed through an overall pattern of the peaks seen in Figure 5(c). These observations indicate a possible formation of a new kind of structure resulting from the attachment of mercury to the MOF. This finding is consistent with the experimental results reported by Wu et al. [75].
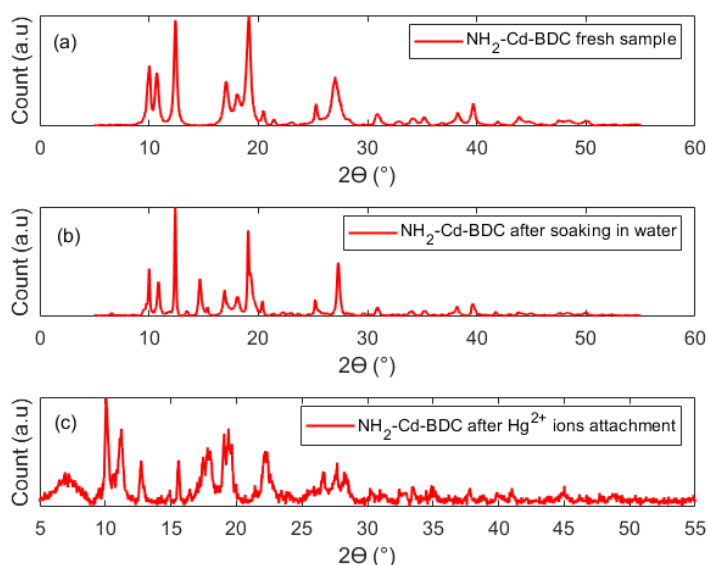
Figure 5: XRD test results for NH_2-Cd-BDC indicating a solid crystalline structure. (a) XRD for a fresh MOF sample. (b) XRD for overnight sample of MOF soaked in water. (c) XRD for a NH_2-Cd-BDC MOF sample after detection of Hg^{2+} ions.

Figure 6 represents the FTIR pattern of the NH_2-Cd-BDC sample. The first peak is obtained at around 3400 cm^{-1}. This peak is indicative of the presence of the hydroxyl

(OH) bond in the tested sample. According to the literature, this peak is attributed to the OH bond stretching, indicating the presence of water (or possibly moisture) in the tested sample [76], [77]. The second peak is observed in the range of 1600-1675 cm^{-1}. This range is attributed to the amide (NH bond) bend majorly along with CO bond bend, C-C bond stretch and N-C bond stretch as reported in the literature [78], [79]. The FTIR results confirm the presence of the amide group, which is important for the purpose of mercury detection, given the high chemical affinity of mercury to the amide, as will be explained further in the coming section. The major peak that is present in Figure 6, is the peak obtained around 1400 cm^{-1}. This peak is attributed to the stretching of the phenol group as reported in literature. Phenol group is found in the structure of the organic linker and possible formation of a standalone phenol in the structure of the MOF [76], [77], [80]. Furthermore, a group of peaks can be observed in the range between 800 cm^{-1} and 400 cm^{-1}. These peaks indicate the stretching of the bonds that exist between the metal ion and the organic linker. For the case of the NH$_2$-Cd-BDC MOF, these bonds connect the cadmium ion and the oxygen ions. Similar observation was previously reported by Wu et al. [81] and Carlos et al [82]. Where in the work of Wu et al. [81] a similar peak at 500 cm^{-1} was found when the cadmium (II) perchlorate hexahydrate was used to produce the metal cluster for the MOF, which is the same metal salt that was used in this work as well. This indicates that when this metal salt is used a certain bond stretching occurs at 500 cm-1 and is indicative of the cadmium and oxygen bond stretching [81].
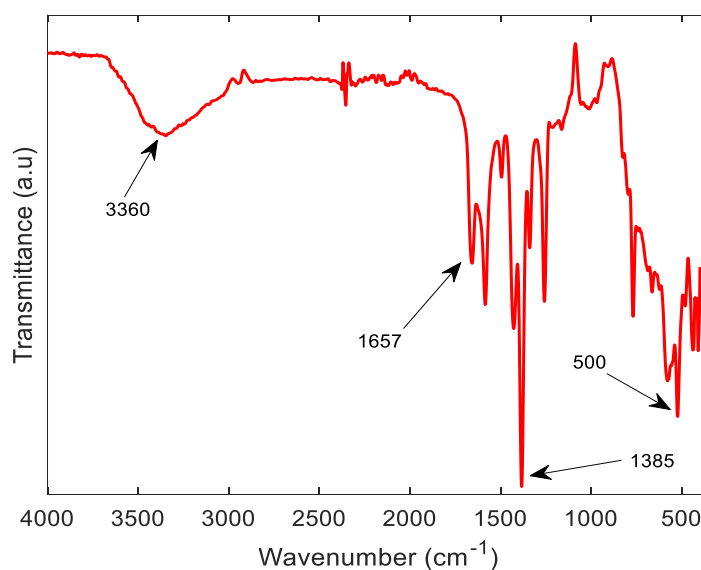
Figure 6: FTIR test results of NH$_2$-Cd-BDC.

33

To gain further insight on the structure of the developed MOF, the SEM test was conducted. The obtained SEM images are displayed in Figure 7. Figure 7(a) shows the results obtained at a magnification of 10 µm and Figure 7(b) presents the results obtained at a magnification of 5 µm. The results of this test confirms again the crystalline structure of the developed MOF as proven by the XRD tests. Furthermore, the SEM pictures reveal that the structure of the MOF is of a sea-shell shape. This founding is rather distinctive because only few MOFs have this unique shape. To the best of the authors' knowledge only the work by Liang et al. [83] reported a similar shape to the current synthesized MOF [83]. This unique shape of the NH_2-Cd-BDC is advantageous in the detection of Hg^{2+} as it provides a large area of pores for the ions to be trapped in [83]. Furthermore, it allows for the direct contact between the amino bond and the Hg^{2+} ions, which further enhances the detection mechanism and allows for the immediate change in the luminescence of the MOF. To further investigate the surface morphology of the developed MOF, at higher magnification and resolution levels, the FE-SEM test was conducted. The images of the FE-SEM test are displayed in Figure 8. Figure 8(a) and Figure 8(b) show the results obtained at a magnification of 1 µm and 500 nm, respectively. The FE-SEM test results reveal the smooth surface of the flake like structure of the main sea-shell particles.
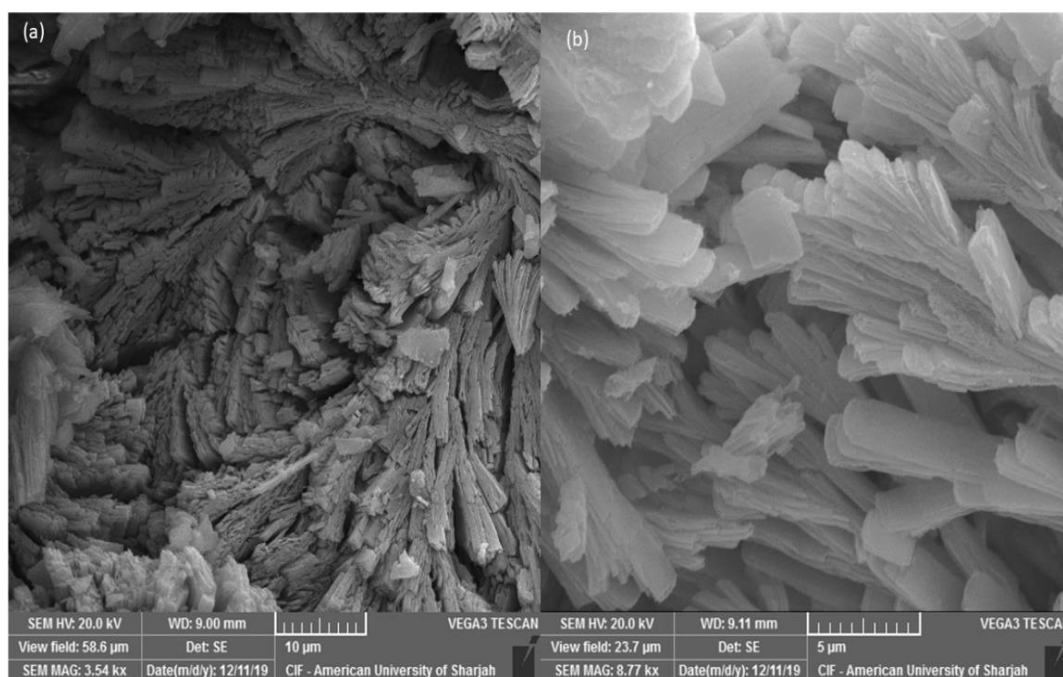
Figure 7: SEM test results for NH_2-Cd-BDC. (a) Test results at magnification of 10 µm and (b) Test results at a magnification of 5 µm.
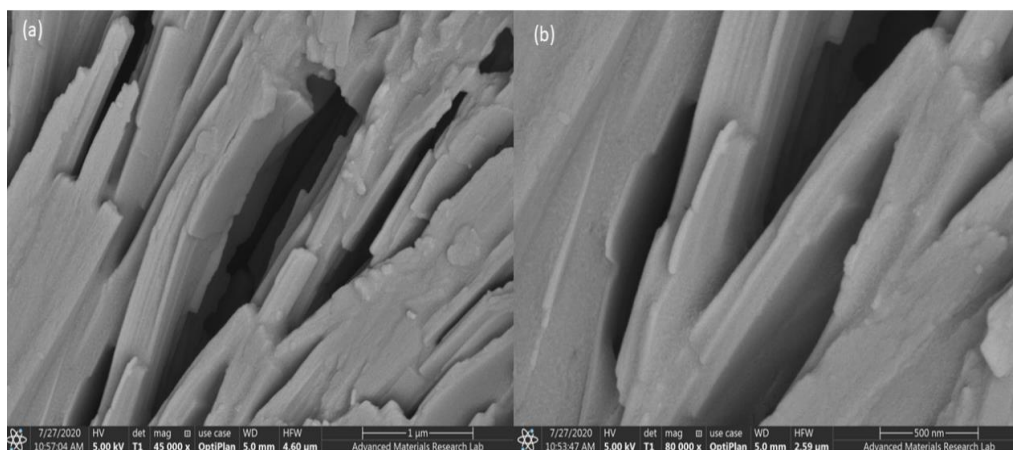
Figure 8: FE-SEM test results for NH$_2$-Cd-BDC. (a) Test results at magnification of 1 µm and (b) Test results at a magnification of 500 nm.
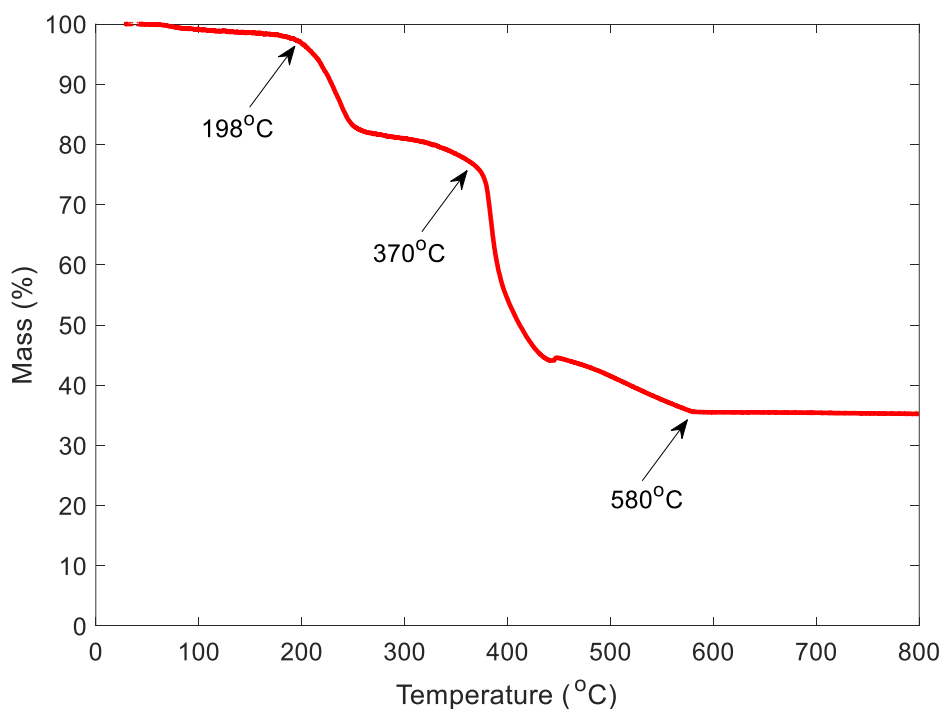
Figure 9: TGA test results for NH$_2$-Cd-BDC showing the mass percentage as a function of temperature.

The thermogravimetric analysis (TGA) was performed on the sample as well to further inspect the thermal stability of the NH2-Cd-BDC MOF. Figure 9 shows the corresponding TGA results, presented as the variations of the mass percentage of the original sample with temperature. The obtained trend indicates that the developed MOF has high temperature stability. The minor drop in the weight observed around 100°C is

associated to the evaporation of water (possibly moisture) and remaining solvent or unreacted chemicals [84]. The first major drops in the mass occur at a temperature of 198°C and then around 350°C, indicating the resemblance and alteration of the polymer bonds in the NH_2-H_2BDC linker [85], [86]. The second major drop in the mass observed at the temperature of 370°C can be explained by the breakage of the backbone of the polymer of the NH_2-H_2BDC organic linker and this is indicative of the loss of thermal stability of the MOF [86]. The drop at around 420°C is mostly attributed to further breakage of side chains and bonds in the 2-aminoterephthalic acid [87]. At 580°C, the curve starts to flatten out indicating that the MOFs structure has lost all its crystallinity [86].

DLS measurements for particle size distributions were also obtained the NH_2-Cd-BDC MOF. The DLS provides the hydrodynamic diameter of the particles suspended in a fluid through the measurement of the speed of these particles. Based on the Brownian motion theory, the smaller particles move at a higher speed than larger particles and with aide of the light scattering technique, the diameter of the particles is determined [88]. The diameter of the MOF particles indicate the adequacy of the MOF for detection purposes. The smaller the particle size of the MOF is, the better is its detectability of ions [89]. The DLS our MOF was recorded and the diameter was found to be 397 nm for NH_2-Cd-BDC. The small diameter of the MOF demonstrate its promising detection ability as the small diameter allows for a higher surface area as mentioned above.

3.2.2. Prospective structure of NH2-Cd-BDC. We use the results obtained from the characterization tests along with the main features of the structure of the organic linker reported in literature to come up with a possible configuration for the NH_2-Cd-BDC MOF structure shown in Figure 10. According to the literature, the NH_2-H_2BDC, which is commercially known as 2-aminoterephthalic acid, consists of a benzene ring that has an amino group (NH_2) attached to it [85], [86]. To this benzene ring, 2 carboxylic acids attachments are present on both sides of the ring [85], [86]. However, deducing the structure for the developed MOF requires deeper analysis of how the metal, which is in our case cadmium, will attach. Based on previously tested and reported MOFs, the metal ion usually binds to the organic linker through forming complex bonds with the oxygen from the carboxylic acid. This was confirmed by the FTIR spectra where a peak was observed at 500 cm^{-1} indicates a direct connection

between the metal ion and the organic linker [81]. Furthermore, MOFs that are aluminum and iron based, as reported in literature, showed that the metal ion usually bonds to the oxygen from the carboxylic acid as stated above [90]. Thus, given the high similarity in the chemical properties of cadmium when compared to aluminum and iron, it is anticipated that the cadmium ion will form a similar bond with the carboxylic acid. Moreover, aluminum, iron and cadmium are all found in the block of transition metals in the periodic table and share similar chemical behavior when it comes to bonding. These metal ions are known to have an electron-rich centers. This center favors an oxidative addition reaction, which in aims at increasing the electron density of the metal [90]. Hence, the cadmium becoming able to bond with more oxygen ions and form the structure found in Figure 10.
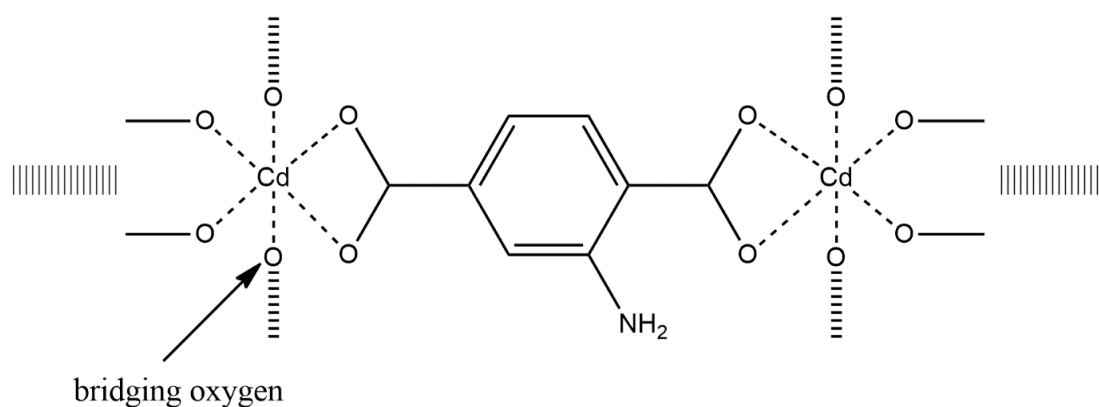
Figure 10: Possible structure of the NH$_2$-Cd-BDC MOF.

3.2.3. Detection experiments. In this section, the detection experiments for the NH$_2$-Cd-BDC MOF will be presented.

3.2.3.1 Detection of mercury. To carry out the mercury detection study, the potential behavior of the NH$_2$-Cd-BDC MOF was investigated in aqeous solutions toward mercury ions follwing the procedure described in the previous section. As displayed in Figure 11, the NH$_2$-Cd-BDC shows a drastic fluoroscence quenching upon the addition of Hg^{2+} into the NH$_2$-Cd-BDC solution. The fluoroscence intensity dropped significantly and immediately from the baseline (denoted by the blue curve in Figure 11) that has a peak with an intensity of 9.75 to 0.75 after the addition of mercury, as indicated by the orange curve in Figure 11. This gives a quenching percentage of 92.3%. Furthermore, it was clearly observed by visual fluoroscence color change of the

37

solution under UV light irrandation (365 nm) as shown in the insert in Figure 11. This fast and strong quenching demonstrates the great property of the MOF in the effective detection of mercury ions. Furthermore, the large drop in the peak, means that the MOF luminscene property is greatly affected by the mercury adsorption phenomenon and the adsorption of the mercury ion causes a major change in the structure of the MOF. Additionally, the large drop in the peak can be associated to the high rate of capturing of mercury ions. It is important to note here that the quenching of the MOF due to mercury absorption happens immediately with no delay at all. This can open the door for the possibile use of the MOF as a promising adsorbent.
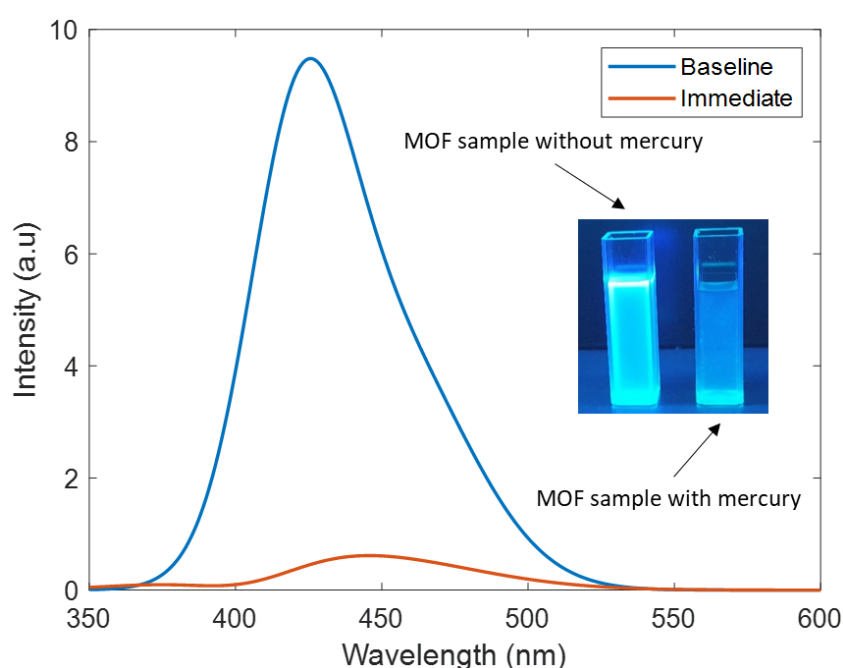
Figure 11: Mercury detection results obtained from the fluoro-spectrometer. The blue curve indicates the baseline reading, which is the MOF original luminescent when added to water. The orange curve indicates the immediate reading after addition of mercury ions to the MOF solution. The concentration of mercury is 200 µM after dilution with the NH_2-Cd-BDC solution. The excitation wavelength was set at 330 nm.

3.2.3.2 Possible mechanism of mercury detection. To explain the quenching phenomena observed in Figure 11, a possible detection mechanism is alluded to. Upon further analyzing how the NH_2-Cd-BDC captures the mercury ions in water, we show in Figure 12 the possible binding mechanism of the mercury ions. According to literature, the NH_2-H_2BDC organic linker is a self-luminescent material that has the amine group in its structure. This amine group presence is of a high importance due to

38

its nucleophilic nature [50], [85]. Given these properties, potential configuration and possible interaction of Hg^{2+} with NH_2-Cd-BDC is illustrated in Figure 12. Based on previously reported studies on detection and trapping mechanisms, the high selectivity of MOF for mercury ions is probably attributed to the three factors. The first factor is the large radius and coordination diversity of Hg^{2+}; in this theory the Hg^{2+} ions attach to the MOF because of the physical properties of the ion possess [91]. The second factor is attributed to the presence of the amino group (NH_2) in the organic linker; these amino groups have nitrogen centers that are classified as soft donor atoms and they increase the affinity towards mercury ions, which are considered to be a soft acid. This is the reason many MOFs that have organic linker consisting of amino groups have high selectivity for mercury ions. The mercury ions have a high affinity towards attacking the amine group with their high nucleophilic property, creating a possible bonding mechanism. This causes the MOF's luminescence to decrease due to the binding and possible disruptions in the electronic configurations as a result of the substitution reaction. This happens when the mercury ions react with the nucleophilic center of the amine group, i.e. nitrogen [50], [51], [91]. As shown in Figure 12, we find that this is mostly a dominant factor due to the presence of the amine group and the favorable attacking phenomena of the mercury ions, which causes the binding and "turn off" of the MOF. The results of the XRD test reported in Figure 5(c) further confirm the second factor analysis. This is due to the appearance of new peaks in the XRD of the MOF after mercury attachment, along with changes in the intensity of the new peak and an overall blunt shape of the peaks. All these changes in the XRD of the MOF after attachment indicate that major structure changes have occurred due to the attachment, which further leads to the conclusion that a new struture is formed. The formation of a new structure is consistent with the mechanism of mercury attachment as explained above and the occurrence of the substitution reaction phenomena. The third factor is the presence of a suflone group, which consists of a sulfur center organic linker [50], [92]. In this research work, we propose that the mercury ions bind to the amino group because of the high chemical affinity present due to the presence of the amino group (nitrogen center theory) along with the fact that mercury ions have their large radius and coordination diversity contributing to the high selectivity. Additionally, we propose the unfavorability of the theory of sulfone presence (sulfur center theory). This binding results in an alteration of the physical and chemical property of the organic linker. This

alteration will further result in the change of the luminescence property of the MOF due to the physical change in the organic linker [50], [51]. Thus, upon the capture of mercury ions quenching of the MOF can be immediately observed and change in fluorescence can be detected. In addition, we note that the bridgings between metal nodes are mostly attributed to the oxygen atom from the $(ClO_4)^-$, which is in good agreement with previously published MOFs composed of $Cd(ClO_4)_2$ metal clusters [81], [93]. Figure 12 below shows the possible coordination of the multi-layer MOF with mercury attachment, where the bridging oxygen is indicated. This shows a possible coordination of the MOF with the use of the $Cd(ClO_4)_2$ metal salt for obtaining the Cd-based MOF.
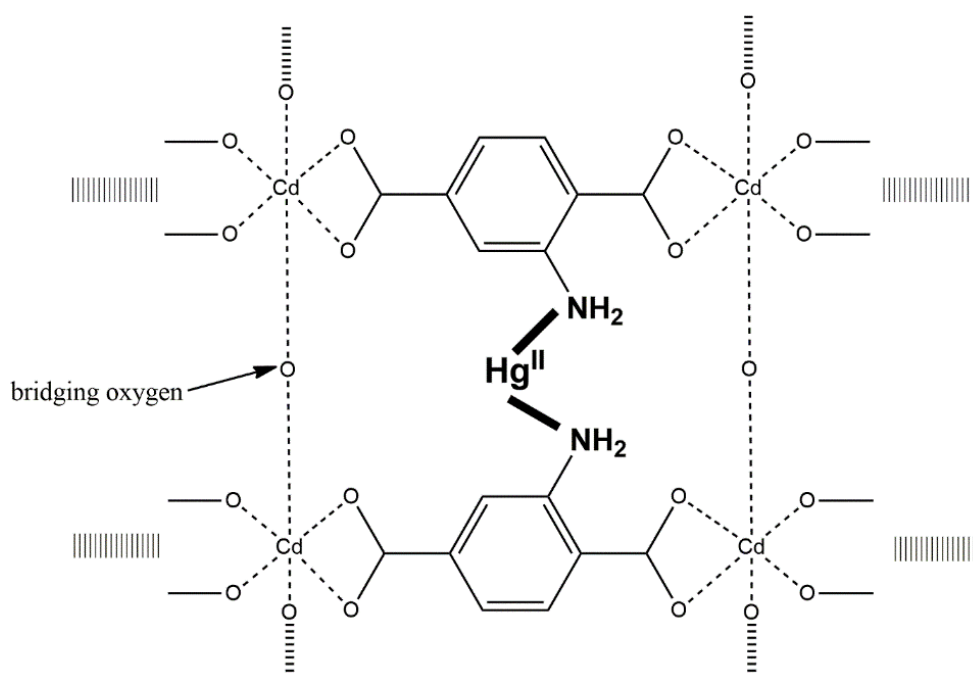
Figure 12: Possible attachment configuration of the mercury ions bonding to the amine group, causing the quenching of the NH_2-Cd-BDC.

3.2.3.3 Single ion comparison. Next, to examine the selectivity of the NH_2-Cd-BDC for mercury over other ions, a single ion test was conducted for a wide range of ions that could be potientally present in water environment. For instance, calcium, sodium and potassium are readily avaliable in almost every water source, as they are prime minerals needed by living organsims [94]. Hence, their presence in water is inevitable and it is important that the proposed MOF is insensitive to them so that the adsorption will be exclusively performed on mercury. Moreover, chromium, lead and

cadmium ions are considered as toxic heavy metals and their production from industries is intense [95], [96]. As such, these ions were tested as well to ensure that the MOF remains selective to mercury when it is placed in an environment that contains these ions. Furthermore, we extended our experimental study to include iron ions given the findings previously reported by Liu et al. [51] revealing that certain MOFs that were originally designed for mercury detection have a capability to detect iron ions as well [51]. Similar analogy was considered to include the copper ions in the present experimental study. As reported by Razavi et al. [97], copper ions have a tendency to be problematic when the MOF devised for mercury sensing is deployed in a water containing copper ions [97]. The quenching percentages obtained from single ion tests for NH_2-Cd-BDC to investigate its selectivity in prescence of different metal ions are shown in Figure 13 and Figure 14. The exeprimental results indicate the superiority of the NH_2-Cd-BDC in detecting mercury as shown from the noticeable decrease in the luminescence leaving only 7% intensity compared to the baseline. On the other hand, the single ion tests revealed that the other toxic heavy metals, chromium and lead have less effect on the luminscene of the MOF. Indeed lead and chromium left 84% and 55% of the MOF luminscene, resepctively. Also, cadmium, which is another toxic heavy metal, showed no effect on the quenching of the intensity of the MOF. The MOF remained luminscent indicating total insensitivity towards it. Additionally, for sodium, calcium and potassium the MOF showed no adsorption capability as indicated by the obtained 100% luminscene percentage. This indicates that the MOF has poor selectivity to these ions that are readily avaliable in water. The experimental observations related to the analysis of iron and copper ions are consistent with those reported in the literature [51], [97]. They found that these ions can cause quenching in the intensity of the MOF. However, the results of quenching are not as high as the one induced by the exposure to mercury. This indicates better selectivity of the MOF to the mercury ions in an environment where all the after mentioned ions may co-exist. These results demonstrate the suitability of the developed MOF for mercury detection in aqueous media, even in the prescence of other ions. We note that the experiments were conducted in duplicate and repeated three times to confirm reproducibility. The maximum relative standard deviations (RSD) was found equal to 8%.
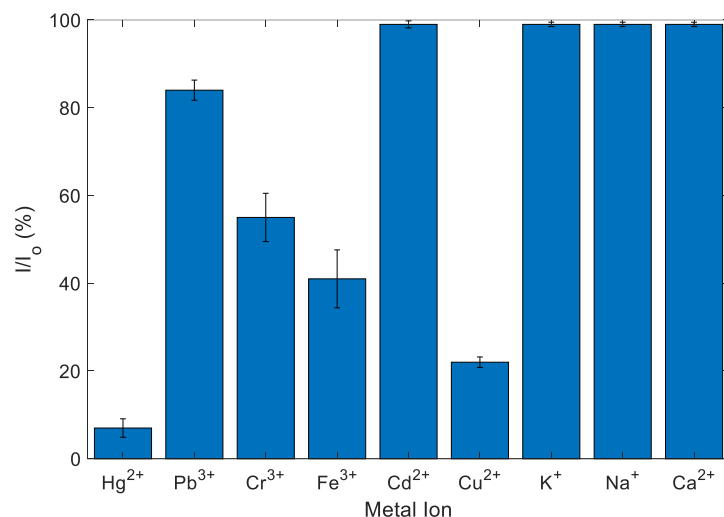
Figure 13: Single ion test for NH$_2$-Cd-BDC to investigate selectivity. All ions were tested at a concentration of 200μM.
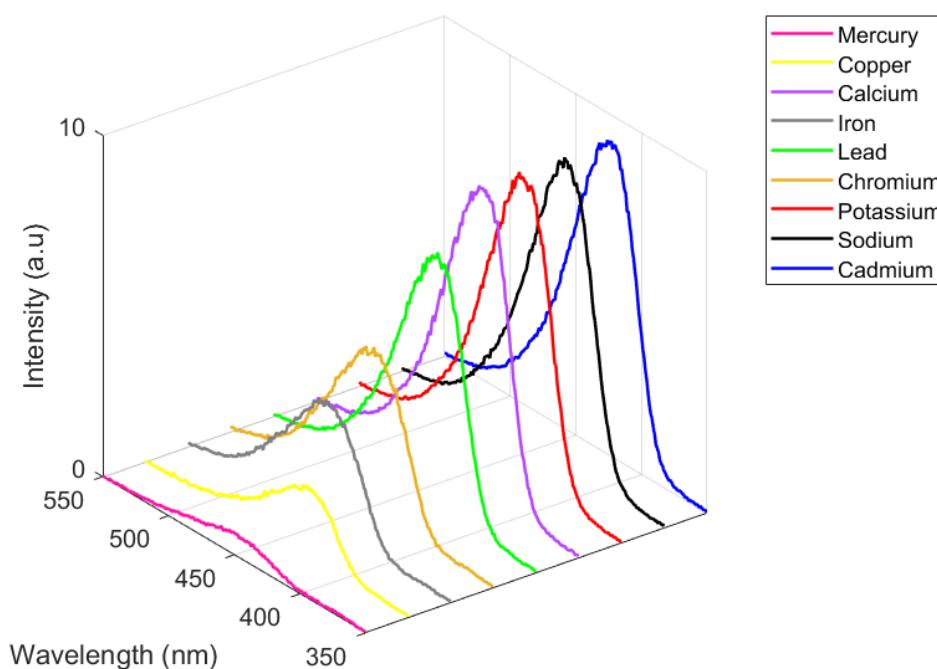
Figure 14: 3D representation of the intensity of the MOF when exposed to different ions (single ion detection tests) done for different metal ions. All ions were tested at a concentration of 200μM.

3.2.3.4 Determination of limit of detection (LOD). The limit of detection (LOD) of the MOF, indicating the lowest mercury concentration that can be detected, constitues an important performance metric that needs to be assessed. To do so,

different concentrations of mercury solutions were tested with the NH$_2$-Cd-BDC ranging from 5 µM to 1000 µM. We note that these concentrations are those of the prepared solutions and not of the tested solutions, as the solutions get diluted upon performing the test. The adjusted concentrations after dilution are calculated to be from 1 µM to 200 µM (denoted by C$_{Hg}$ thereafter). This allows for a better mimic of real life situations and enables to analyze lower concentrations of the sensing elements as needed to properly identify the LOD of the MOF. We plot in Figure 15 the variations of the intensity with the wavelength of the tested concentrations as obtained from the fluorescence spectroscopy. Again, the baseline presents the solution including only the MOF. As expected, a decrease in the major peak is obtained when increasing the mercury concentrations. Of interest, the results show that the MOF was sensitive to mercury until a concentration of mercury of 1 µM, where the obtained curve approaching the baseline curve. Other concentrations fall in a descending order upto the 200 µM concentration. These results gave an indication of the limit of detection of the MOF, which is evaluated by producing the Stern-Volmer graph.
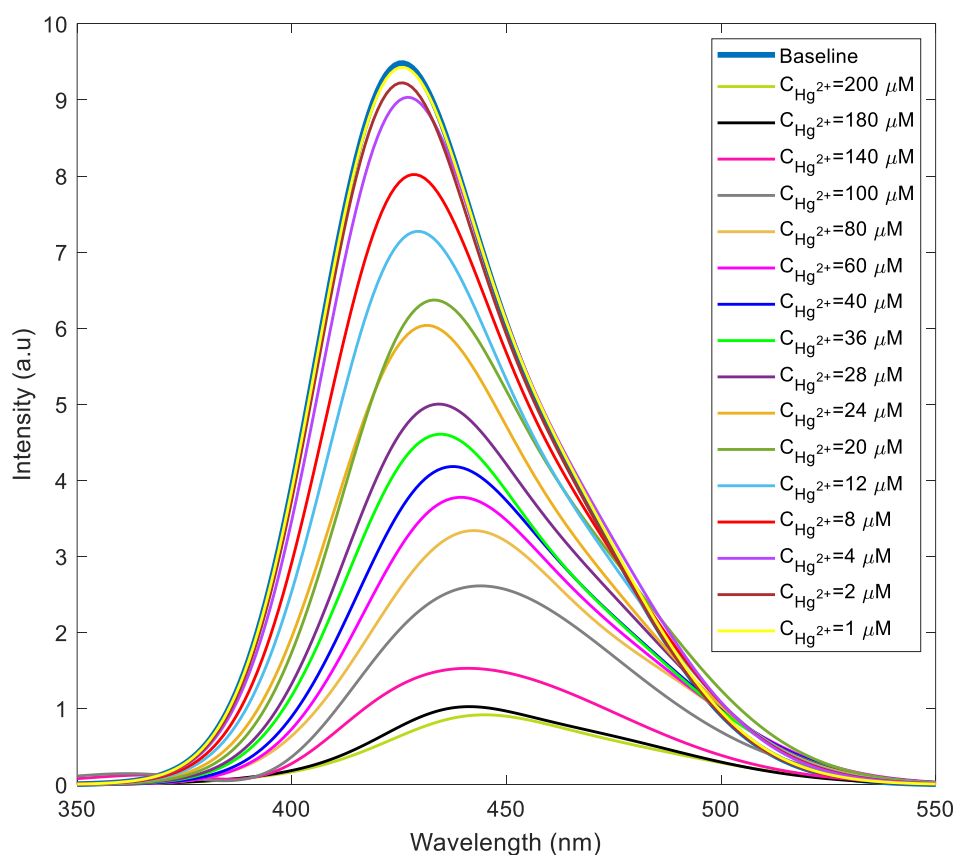
Figure 15: Mercury detection results of NH$_2$-Cd-BDC for different concentrations of mercury ranging from 1 µM to 200 µM.

43

Next, we use the variations of the peak intensity shown in Figure 15, for low mercury concentrations to produce the Stern-Volmer graph displayed in Figure 16. Four mercury concentrations were studied (1 µM, 2 µM, 8 µM and 20 µM). The equation obtained from the best linear fit line relating the relative change in the intensity to the mercury concentration is y=0.028x + 0.033 and the R^2 value was found equal to 0.99 indicating a linear trend. The slope of the best linear fit curve gives the K_{sv} value, which was found to be 28.0×10^3 M^{-1} (the Stern-Volmer constant) [50]. We note that the obtained value of the K_{sv} is comparable those reported in literature, such as the one found by Wu et al. ($K_{sv} = 4.3 \times 10^3$ M^{-1}) [81]. Using this constant and as discussed in the testing section, the LOD was calculated and found equal to 0.58 µM. This value of LOD represents the actual limit of the NH_2-Cd-BDC to detect mercury. This value of LOD obtained shows the high potential use for the NH_2-Cd-BDC MOF as a mercury detector.
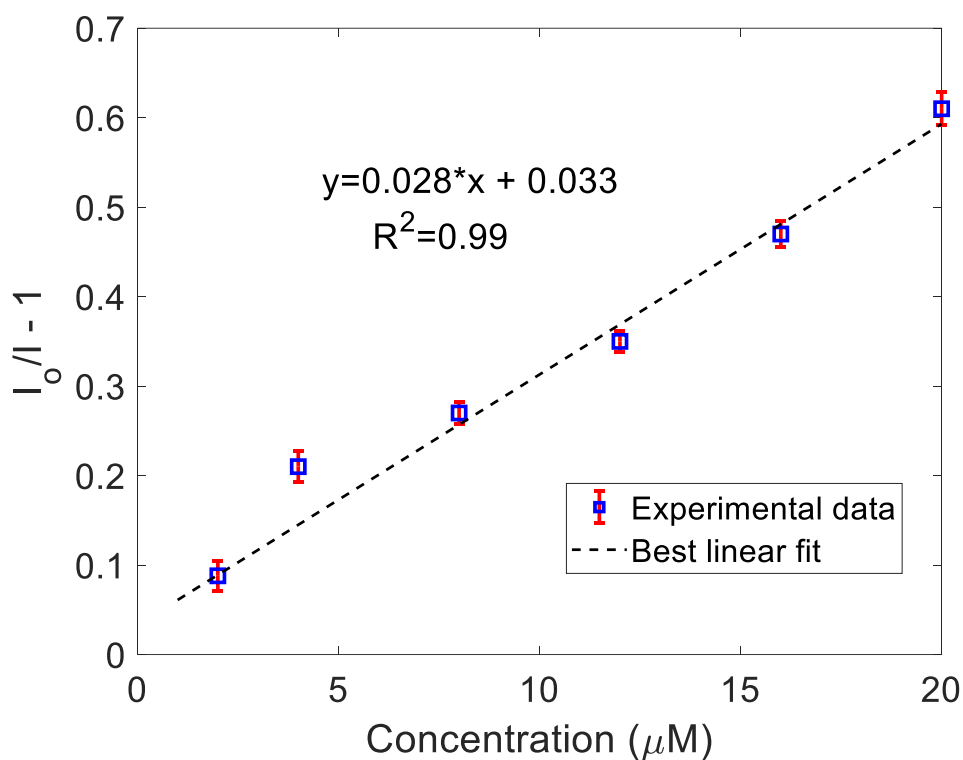
Figure 16: LOD determination using the Stern-Volmer fitting curves method for mercury. Error bars represent the standard deviation of 6 trials while the points represent the average of these trials.

The LOD of the MOF to iron is also determined following the procedure applied for merucry. Again, solutions with concentrations varrying from 20 µM to 1000 µM

were prepared for this test and upon adding to the MOF solution, the concentrations were adjusted in the calculations to represent the real concentrations, which are from 4 µM to 400 µM. Figure 17 shows the results of the MOF quenching due to the different concentrations of the iron used. We stopped at 4 µM upon noticing from the experiments that the MOF is not responsive to concentrations below than 4 µM. On the other hand, the experiments revealed that our MOF responds to mercury at lower concentrations (1 µM). This finding demonstrates further the suitability of the developed MOF for mercury detection, even in presence of other heavy metals. The LOD was also determined using the Stern-Volmer method as performed for the mercury. Figure 18 shows the results for the Stern-Volmer fitting curve used for the iron LOD determination. The iron LOD was found equal to 1.59 µM. This value is higher than the LOD obtained for mercury. This indicates the superior NH_2-Cd-BDC selectivity of mercury ions.
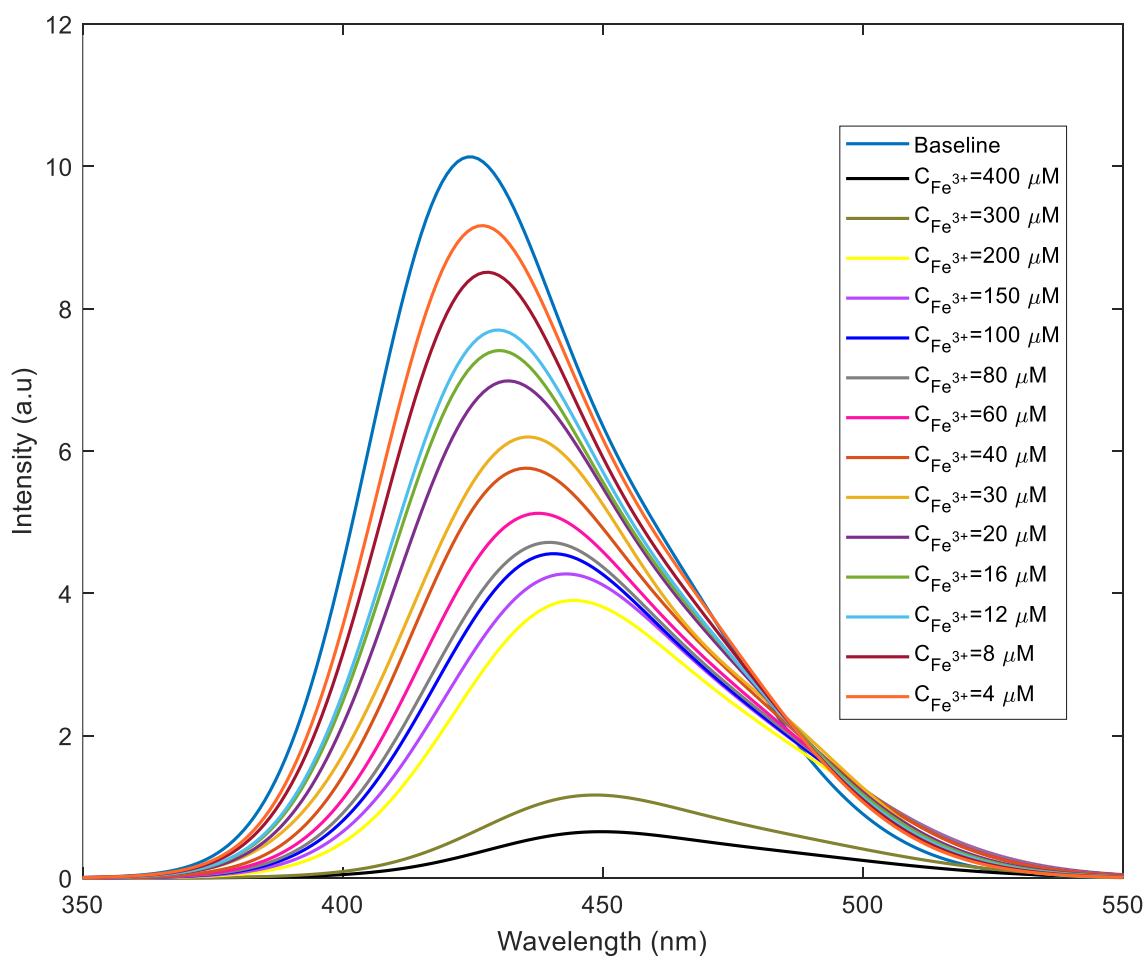
Figure 17: Iron detection results of NH_2-Cd-BDC for different concentrations of iron ranging from 4 µM to 400 µM.

$$y = 0.024 * x + 0.023$$
$$R^2 = 0.9919$$
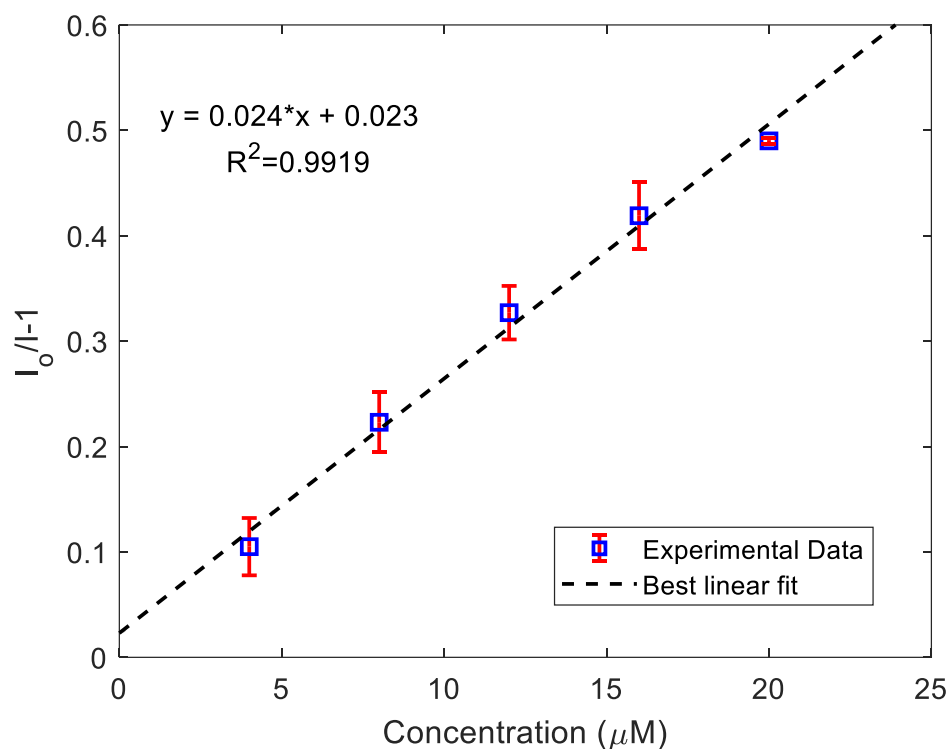
Figure 18: LOD determination using the Stern-Volmer fitting curves method for iron. Error bars represent the standard deviation of 3 trials while the points represent the average of these trials.

Table 1 compares limit of detection of different sensors for Hg^{2+} ions along with their synthesis mechansim as reported in literature. The comparison includes several other factors besides limit of detection. When comparing the obtained LOD to those reported in the literature, the present Cd-based MOF presents a comparable value that is even lower than other reported MOFs. For instance, the LOD of the Zn-based MOF proposed by Razavi et al. [97] was found equal to 1.8 µM. The Co(II)-based MOF developed by Su et al. [56] had a LOD of 4 µM. Furthermore, our proposed MOF was observed to be competitive with other material detectors such as Coumarin based probes (0.12 µM) [22] and Gold nanorods embedded in a functionalized silicate sol-gel matrix (0.317 µM) [98]. This indicates that the proposed MOF can be used as a promising sensor candidate for mercury detection given the luminescence property that provides a distintive feature that allows for the Cd-based MOF to carry out the detection in a cost effective manner. Furthermore, the facile microwave synthesis posses an extra advantage as an eco-friendly sythensis route for large scale industrial application.

Table 1: Capabilities and features of materials proposed for mercury detection: comparison with the proposed MOF.

Detector Material	Synthesis technique (Time in hours)	LOD (μM)	Luminescent	Selectivity
NH$_2$-Cd-BDC (this research)	Microwave (1.25 hours)	0.58	Yes	# of ions tested with: 9 Possible competition: Fe^{3+} and Cu^{2+}
$\{[Co_2(L)(hfpd)(H_2O)]\cdot 1.75H_2O\}_n$ [56]	Hydrothermal (72 hours)	4	Yes	# of ions tested with: 18 Possible competition: Fe^{3+} and Ag$^+$
Coumarin based probes [22]	Heating under N$_2$ (24 hours)	0.12	Yes	NA
NH$_2$-MIL53(Al) [50]	Solvothermal (6 hours)	0.15	Yes	# of ions tested with: 11 Possible competition: Pb^{2+}
Zn-based MOF [97]	Sonication (1 hour)	1.8	Yes	# of ions tested with: 16 Possible competition: Cu^{2+}
Gold nanorods embedded in a functionalized silicate sol-gel matrix [98]	NA	0.317	No	# of ions tested with: 11 Possible competition: Mg^{2+}

3.2.3.5 Competitive environment detection. To further prove the selectivity of the developed MOF and confirm the results obtained from the single ion tests, a competitive environment detection test was carried out. The same ions used in the single ion test were considered in the competitive environment tests, while doubling their concentration to 400 µM and keeping the concentration of mercury equal to 200 µM. Details on the solution preparation and testing procedure are provided in the testing section. The results of the competitve environment tests are shown in Figure 19. The experimental results clearly demonstrate the superiority of mercury detection in comparison to other ions such as the sodium, potassium, cadmium and calcium. These four ions showed no adsorbance to the MOF even when doubling their concentration. Also, when the mercury was added, the quenching occurred with the lumincescene remaining for all at the same level and equal to 49%, except in the case of cadmium, where it dropped to 17%. The larger drop, observed for the case of the cadmium, can be attributed to the fact that cadmium ions are bigger than the pores of the MOF resulting in the pores being unoccupied and allowing for mercury ions to better infiltrate the MOF's structure. The size of the sodium, potassium and cadmium ions allow them to block some of the pores of the MOF and that results in a higher quenching level (49%) [50]. For the chromium, the luminscene left after adding the MOF was 37% but when the mercury was added, the luminescence dropped to 9%. Similarly for lead, the luminescence dropped to 52% but when after the addition of mercury it was reduced to 14%. These results indicated that the MOF captured some of the chromium and lead ions initially. However, when the mercury ions were added, the MOF still captured the mercury ions and showed further quenching. This demonstrates that although the MOF had some affinity towards the chromium and lead, its high selectivity still stood when the mercury ions were added. The only ions that showed unfavorable results were the iron and copper ions. In the case of iron ions, the double concentration caused the luminescence remaining to drop to 17% and when the mercury was added, the luminescence remaining percentage further dropped only to 15%. This result means that the iron can affect the NH_2-Cd-BDC selectivity. However, the MOF still showed selectivity to the mercury ions when they were added through two indications: (i) the slight drop in the percentage; (ii) the shifting of the curve after the mercury ions were added. These observations are in agreement with other observations found in literature on the same tests [51]. Similar to the iron ions, copper ions caused high quenching in

the MOF at double concentration, dropping the quenching percentage to 16%. However, when the mercury was added further quenching occurred and dropped the percentage to 12%. These results are consistent with the findings of Razavi et al. [97], who reported that copper ions tend to be detected by MOFs designed for mercury detection. Nevertheless and similar to the iron ions, the selectivity towards mercury is proved by noticing a shift in the curve and the additional slight drop in the quenching percentage. These two results indicate that even when the MOF was detecting iron and copper ions, the mercury ions selectivity is still maintained because of the nitrogen center theory stated above. Additionally, for further confirmation that the effect of iron ions shall not disturb the MOFs potential in working in the open water sources, it was investigated and found out the natural minerals of water do not include iron [99].
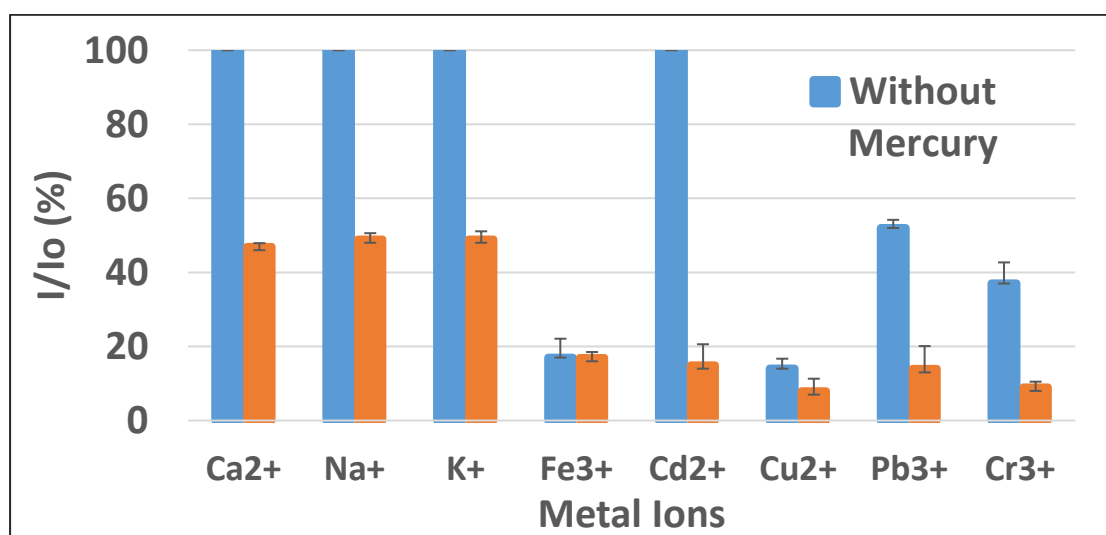
Figure 19: Quenching percentages obtained from competitive environment tests for NH2-Cd-BDC to investigate its selectivity in presence of different metal ions. The concentration of mercury is set equal to 200 µM and the concentration of all other metals ions is set to 400 µM.

3.3.   Conclusion

In this chapter, we presented the development a novel MOF, namely NH_2-Cd-BDC to selectively detect mercury in aqueous environments. This MOF comprises cadmium ions as metal cluster and 2-aminoterephthalic acid as organic linker. It was successfully synthesized using microwave oven, enabling fast and cost-effective synthesis procedure. To inspect its crystalline structure and thermal stability, several characterization tests were conducted, including XRD, FTIR, FE-SEM, TGA and SEM.

These tests revealed that the developed MOF has a crystalline sea-shell shape with high thermal and water stabilities. Also, the performed characterization tests revealed that the cadmium ion undergoes an oxidative addition reaction. This allows it to increase its oxidation state and form a linkage with the organic linker at the oxygen in the carboxylic acid group. Forming a similar structure to what is seen in aluminium and iron based MOFs. Furthermore, the capability of the MOF to detect mercury in aqueous media was qualitatively and quantitatively assessed. Indeed, the MOF showed excellent detection of Hg^{2+} ions with 92.3% quenching of fluorescence intensity with respect to the baseline solution (MOF soaked in water without mercury). Of interest, the MOF showed no detection or significantly low detection for other metal ions such as chromium, cadmium, lead and iron when it was tested singularly and competitively with the mercury ions. The NH_2-Cd-BDC detection limit was also quantified and found equal to 0.58 µM for mercury ions. The consistency of the experimental results was verified by conducting six replicates. Based on the competition results, the MOF was found to be slightly sensitive to iron. As such, the experimental investigation was extended to analyse the iron detection of the developed MOF. The LOD of iron for the NH_2-Cd-BDC MOF was computed and found equal to 1.59 µM. This value is almost three times that obtained for the mercury. This further confirms the high selectivity of mercury in the case of co-existence of both ions in a water body. The experimental results demonstrate the potential use of the developed MOF as coating material of MEMS devices for chemical sensing applications.

Chapter 4. Comparative Study between NH₂-Cd-BDC MOF and Other Amino-functionalized MOFs

In this chapter, a comparative analysis is conducted between the NH$_2$-Cd-BDC novel MOF presented in chapter 3 and other amino-functionalized MOFs that were reported in the literature. Using the same organic linker of NH$_2$-H$_2$BDC, three metal clusters were used which are, Al^{3+}, Zr^{2+} and Fe^{3+}. The obtained MOFs are NH$_2$-MIL53(Al), NH$_2$-UiO-66 (Zr) and NH$_2$-MIL88(Fe), respectively. The MOFs were prepared following the synthesis techniques reported in the literature with some modifications. Given its fast heating process, all the MOFs were synthesized using the microwave-assisted synthesis technique. The present analysis includes mainly a comparison between the performance of the four MOFs in terms of their crystalline structure, thermal stability and capability to detect metal ions in both single and competitive heavy metal ion in an aqueous environment.

4.1. Materials and Methods

The synthesis procedure of the NH$_2$-Cd-BDC MOF, the testing procedure and calculation steps, the equipment used and the characterisation test procedures are described in Chapter 3 above. In addition, details about the NH$_2$-Cd-BDC MOF also given in Chapter 3.

4.1.1. Materials. The chemicals used in the comparative study were purchased from Sigma Aldrich through its local supplier in the UAE, LabCo. These chemicals are cadmium (IV) perchlorate hexahydrate: Cd(ClO$_4$)$_2$ • 6H$_2$O, Iron (III) chloride hexahydrate: FeCl$_3$•6H$_2$O, aluminum chloride: AlCl$_3$•6H$_2$O, zirconium (II) phosphate: Zr(HPO$_4$)$_2$•2H$_2$O, terephthalic acid: NH$_2$-H$_2$BDC, dimethylformamide (DMF): C$_3$H$_7$NO, methanol: CH$_3$OH, hydrochloric acid: HCl, sodium hydroxide pellets: NaOH and mercury (II) nitrate monohydrate: Hg(NO$_3$)$_2$ • H$_2$O. All materials were used without further modification with the only exception being for the hydrochloric acid (HCl) which was diluted to match the required concentration of 2 M from its original concentration of 10 M.

4.1.2. Synthesis of MOFs. The synthesis of the NH$_2$-Cd-BDC MOF can be referred to from Chapter 3. For the preparation of the NH$_2$-MIL88(Fe) MOF, the same synthesis procedure was followed as reported by Zhang et al. [50] except for the

following modifications. First, 0.374 gram of $FeCl_3 \cdot 6H_2O$ was dissolved in 30 ml of DMF along with 0.251 gram of NH_2-H_2BDC. Then the solution was stirred for 2 hours to ensure complete homogeneity. We note that unlike the work of Zhang et al. [50] who used the conventional solvo-thermal method, the synthesis of the aforementioned MOF was carried out using microwave irradiation as a facile ecofriendly synthesis technique. The solvo-thermal heating technique, which required heating at 120°C for 20 hours, was replaced with the use of microwave irradiation for 60 minutes at 135°C and 800 W. Similarly, the NH_2-MIL53(Al) was synthesized using the procedure reported by Zhang et al. [50] with some modifications. 0.543 gram of NH_2-H_2BDC was added to 30 ml of deionized water and 0.4 grams of NaOH palettes were added. The pellets were added for dissolving the NH_2-H_2BDC in the DMF [100]. The mixture was sonicated for 30 minutes after which 0.724 grams of $AlCl_3 \cdot 6H_2O$ were added to the mixture. Another sonication step was performed for 30 minutes and then the solution was transferred into the microwave at 120°C for 45 minutes at 700 W. In the work of Zhang et al. [50], the synthesis was carried out using solvo-thermal technique which required heating at 150°C for 6 hours. For the synthesis of the NH_2-UiO-66(Zr) MOF, we followed the procedure reported by Wang et al. [101]. Where 0.182 gram of NH_2-H_2BDC was dissolved in 25 ml of DMF. After complete dissolving of the organic linker, 0.654 of $Zr(HPO_4)_2 \cdot 2H_2O$ was added. The mixture was stirred for 5 minutes to ensure complete dissolving. Similar to the work of Wang et al. [101], the MOF synthesis was conducted using microwave-assisted heating process while changing the microwave settings. The change in the settings was due to the large difference between their microwave used and the one used in this research. In this study, the microwave was set at 125°C for 30 minutes at 700 W.

4.1.3. Characterization. The details about the characterization tests equipment and settings are given in Chapter 3. In this chapter, the characterization tests were conducted for as-synthesized MOFs samples as well as samples of the MOF after mercury adsorption. The preparation of the MOFs after mercury adsorption was performed as follows: 30 mg of the MOF was added to a 25 ml of mercury solution that has a concentration 1000 µM. The mercury solution with MOF was left to be stirred for 3 hours and then left to dry in the oven at a temperature of 100 °C for 1.5 hours. The characterization tests were conducted as presented in Chapter 3 and some FE-SEM images were generated with further magnifications.

4.2. Results and Discussion

4.2.1. Characterization. In this section, the characterization of the MOFs will be presented.

4.2.1.1 XRD. The XRD test was performed on the MOFs before and after their exposure to mercury and as shown in Figures 20. Blue curves denote the results obtained for the fresh sample while red ones correspond to the XRD results of the MOFs after mercury attachment. Clearly, NH_2-Cd-BDC, NH_2-MIL53(Al) and NH_2-UiO-66(Zr) are all crystalline with well-defined and sharp peaks as shown in Figure 20 (a), (b) and (c), respectively. On the other hand, Figure 20 (d) reveals that the Zr-MOF is amorphous. In general, fresh sample exhibit larger relative intensity compared to that obtained after mercury attachment, and there is a noticeable right shift (towards higher angles) in the peaks with mercury adsorption. The uptake of the Hg^{2+} ions into the structure causes the original MOF structure to undergo these physical changes as Hg^{2+} intercalates between original grains [50], [51].
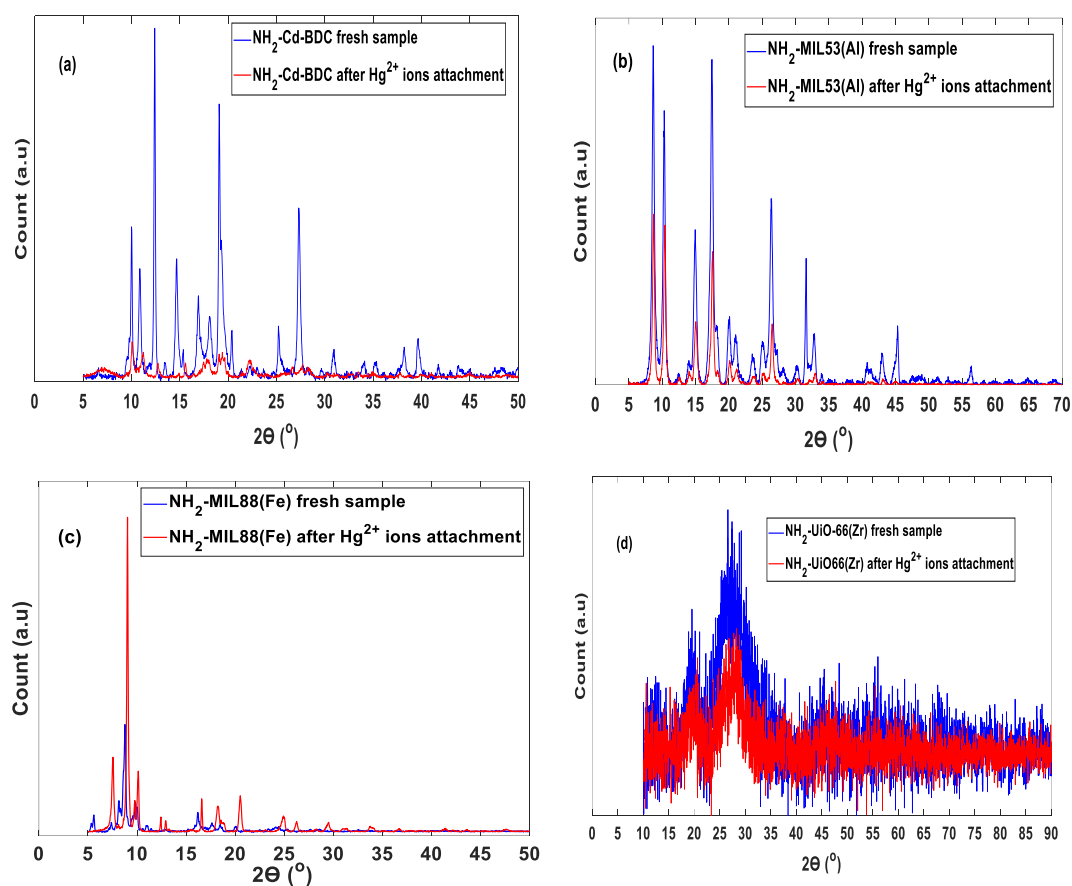
Figure 20: XRD results for the MOFs (a) for NH_2-Cd-BDC MOF, (b) for NH_2-MIL53(Al), (c) for NH_2-MIL88(Fe) and (d) for NH_2-UiO-66(Zr).

The fresh samples of the NH_2-Cd-BDC MOF have XRD graphs (blue curve of Figure 20 (a)) showing crystalline structure with sharp peaks at $2\theta = 13°$, $19°$ and $27°$. The crystalline structure of this MOF undergoes noticeable changes after mercury exposure to mercury ions as can be seen in Figure 20 (a). Moreover, the intensity of the peaks has significantly decreased compared to those of the fresh sample. Interestingly, some of the original peaks have disappeared (e.g. peaks at $2\theta = 27°$, $37°$ and $39°$). This indicates the damage to certain areas of the MOF and the MOF's surface was covered partially with adsorbed mercury [102]. As a general observation, it is evident that the MOF structure undergoes major changes in its structure when mercury is adsorbed. This is mostly attributed to the reaction taking place between mercury and the MOF, specifically the amine group in the MOF. As mentioned above in Chapter 3, the nucleophilic nature of the amine group causes a major attraction point for mercury. Upon this attraction, the reaction happens where the mercury binds to the MOF through attaching to the amine group. Therefore, this causes major structural changes which results in major properties changing and altering [50], [103].

As for the NH_2-MIL53(Al) MOF, the XRD results in Figure 20 (b) (blue curve) in good agreement to those reported in the literature [50]. The crystalline structure of NH_2-MIL53(Al) is characterized by having several peaks due to the coordination and bonding order of the aluminum ions with the organic linker [103]. This structure remains maintains its crystallinity with mercury uptake, shown as the red curve of Figure 20 (b). However, it is clear that the adsorbed mercury has adversely affected the peak intensity and also caused a right shift of these peaks. Furthermore, some peaks from the fresh sample have disappeared (e.g. peaks at $2\theta = 30°$, $40°$, $42°$ and $45°$).

Figure 20 (c) shows the XRD results obtained for the fresh sample of the NH_2-MIL88(Fe) MOF. Again, the high crystallinity observed in the blue curve of Figure 20 (c) is in good agreement with the results reported in the literature [50]. Unlike the NH_2-Cd-BDC and the NH_2-MIL53(Al), NH_2-MIL88(Fe) is distinguished by a sharp peak at small angles at $2\theta = \sim9°$. One the other hand and contrary to its counterparts discussed earlier, mercury adsorption causes an amplification of the peak intensity (as revealed by the red curve of Figure 20 (c)). We can also observe the pertinent right shift in the peak location similar to Cd-MOF and Al-MOF. There are also few peaks appearing at higher angles that are attributed to the mercury attachment impact on the MOF.

Finally, for the NH$_2$-UiO-66(Zr) MOF, a good agreement with the results reported by Fu et al. [104] is confirmed. This MOF is known to be amorphous especially due to the high temperature synthesis route. The microwave-assisted synthesis requires the exposure to high temperatures that alter the microstructure of the MOF. This is in agreement with findings reported in literature, where when the synthesis of the MOF happens at a high temperature, the structure changes its crystallinity degree and becomes completely amorphous [104]. For the XRD results shown in Figure 20 (d), the major peak is observed at around $2\theta = 25°$-$30°$. This is the only major peak that can be observed from the figure. Similar to the rest of the MOFs, the peak intensity undergoes a decrease due to mercury attachment similar to the rest of the XRD pattern. This is because the addition of mercury causes the MOF to change its structure and alters its bonds.

4.2.1.2 FTIR. The FTIR test is conducted to further investigate the structure of the MOF and get a better insight on the mercury interaction with surface of the MOF. These peaks are often evidence for the existence of certain bonds. The FTIR results are displayed in Figure 21. The blue curves denote the FTIR of the pristine samples of MOFs while the red curves represent results after mercury adsorption. All FTIR results obtained for the four MOFs under investigation contain a peak at around 1750 cm^{-1} which is indicative of the presence of the expected N-H bond being the organic linker used in all four MOFs with the NH$_2$ functional group [76]. Additionally, some of the FTIR results for the fresh samples of the MOFs show a peak at around 3600 cm^{-1}. This peak exists due to the water bond indicating a moisture content. This can be observed in the NH$_2$-MIL53(Al) and NH$_2$-Cd-BDC MOF. Similarly, the FTIR results for the MOFs after mercury adsorption do not exhibit the 3600 cm^{-1} peak given that the samples have been dried properly after soaking in mercury solution.

Inspecting the FTIR results of the NH$_2$-MIL53(Al) MOF, found in Figure 21 (b), the pristine sample FTIR is comparable to the one found in literature [103]. The FTIR has two main observable peaks at 1750 cm^{-1} and 1400 cm^{-1}, which represent the presence of the N-H bond and the CH$_3$ bond, respectively. After mercury adsorption, the N-H bond peak undergoes a decrease in intensity. This indicates that the mercury has attacked most of the nucleophilic N-H bonds. The increase in the intensity of some peaks and the evolution of new peaks reveal the successful mercury adsorption, which

alters the MOFs structure. This is consistent with the XRD results presented in Figure 20 (b). As for the NH$_2$-Cd-BDC MOF, Figure 21 (a), the FTIR results exhibit major peaks of N-H bond and the CH$_3$ bond observed at 1750 cm^{-1} and 1400 cm^{-1}, respectively. After mercury adsorption, the N-H bond and the CH$_3$ bonds peaks undergo a significant decrease in intensity. This is mostly associated with the alteration that the MOF undergoes when the mercury is attached to it.

The FTIR results of the Fe-MOF before mercury adsorption are comparable to those found in the literature [50]. The main feature of the FTIR result is the presence of the N-H bond and the CH$_3$ bond at 1750 cm^{-1} and 1400 cm^{-1}, respectively. Figure 21 (c) shows the FTIR result of the Fe-MOF. However, after mercury adsorption, the FTIR curve shows distinctive difference when compared to its counterpart before exposure to mercury. These results further confirms what was concluded from the XRD analysis of this MOF, indicating major changes to the structure of the Fe-MOF after mercury attachment. Also, similar to the XRD results, the peaks show an increase in the intensity, differently from what was observed for the other MOFs. The peaks at 1750 cm^{-1} and 1400 cm^{-1} remain but their intensity increases. As for the Zr-MOF, found in Figure 21 (d), the N-H peak at 1750 cm^{-1} is obtained as well with the appearance of a new peak at 1050 cm^{-1}. This new peak is attributed to the CO-O-CO bond [104]. This is the only MOF observed with such peak and this is mostly due to the coordination and orientation of the MOF. Again, we notice the disappearance of the N-H bond peak after mercury adsorption while the other peaks remain almost unchanged. This indicates that the mercury attachment does not result in major structural changes in this MOF.
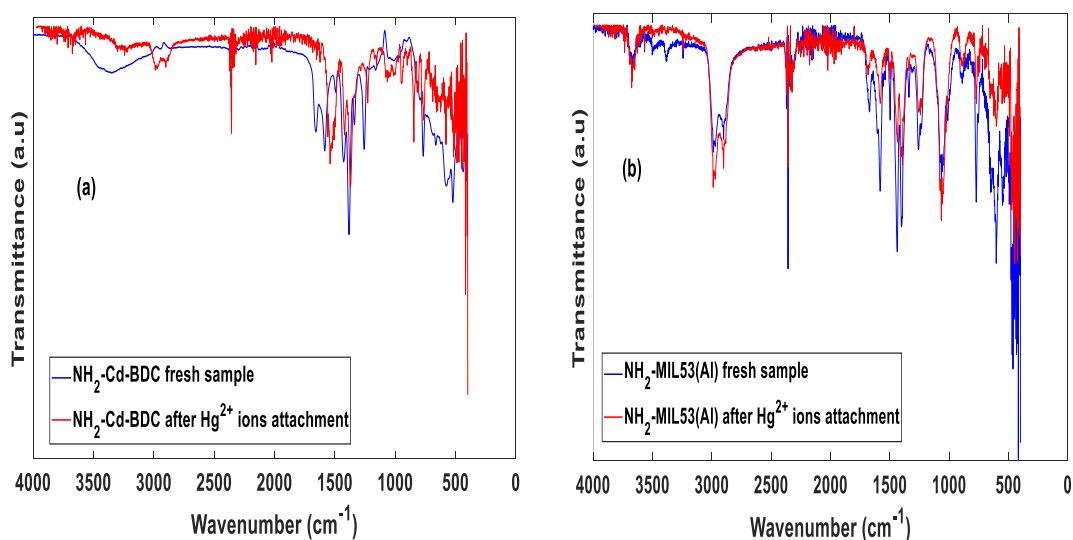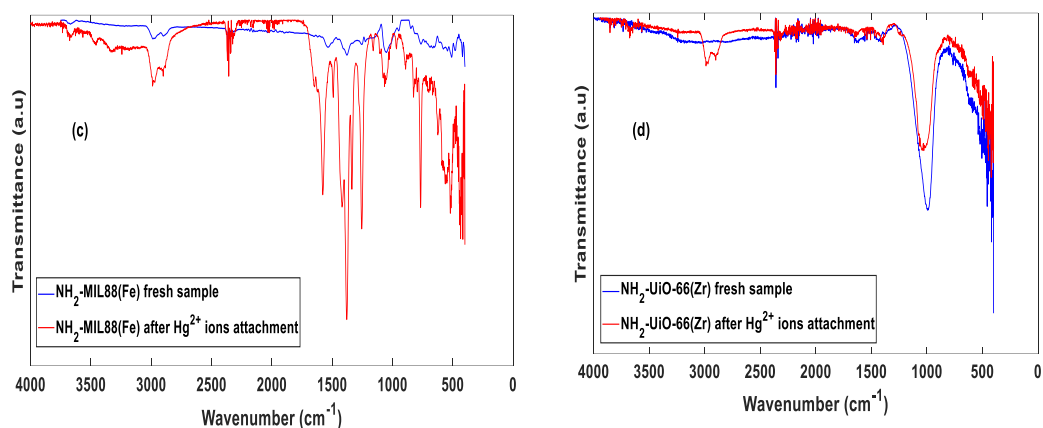
Figure 21: FTIR results for the MOFs (a) for NH$_2$-Cd-BDC MOF, (b) for NH$_2$-MIL53(Al), (c) for NH$_2$-MIL88(Fe) and (d) for NH$_2$-UiO-66(Zr).

4.2.1.3 FE-SEM. The examination of the FE-SEM images of NH$_2$-Cd-BDC MOF after mercury uptake shows a general maintenance of the crystal structure as the MOF retains its distinctive morphology of sea-shell structure with some minor deformities as shown in Figures 22. Figures 22 (a) and (b) show a fresh sample of the MOF, while Figures 22 (c) and (d) show the MOF sample after mercury adsorption. Liang et al. [83] reported similar sea-shell structure for Cd-MOF the organic linker is different [83]. The deformities seen in Figure 22 (c) and Figure 22 (d) explain the peak widening that occurred in the XRD results of Figure 20 (a). This is in accordance to Scherrer equation and the morphological changes that the structure has undergone as explained through the FTIR analysis.
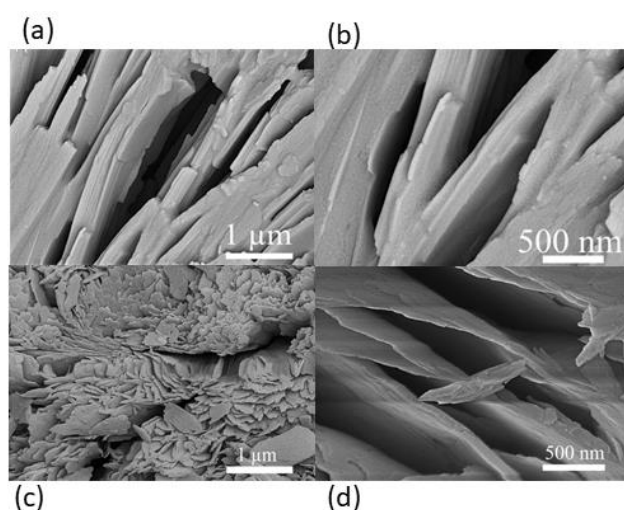
Figure 22: FE-SEM for NH$_2$-Cd-BDC MOF. (a) at 1 µm for fresh sample, (b) at 500 nm for fresh sample, (c) at 1 µm for mercury adsorbed sample and (d) at 500 nm for mercury adsorbed sample.

The FE-SEM images of NH_2-MIL88(Fe) MOF, shown in Figure 23 exhibits a monolithic columnar structure that is fully crystalline confirming further the XRD results displayed in Figure 20 (c). The observed structural features are similar to those reported by Ma et al. [105]. Figures 23 (a) and (b) show a fresh sample of the MOF, while Figures 23 (c) and (d) show the MOF sample after mercury adsorption. The mercury uptake has caused noticeable deformation at the center of these column, which explains the missing peaks in the XRD graphs. These deformations seem to have moved the crystallographic planes in unison and thus have resulted in the increase in XRD peak intensity as shown in Figure 20 (c) compared to the lower peaks of pristine samples.
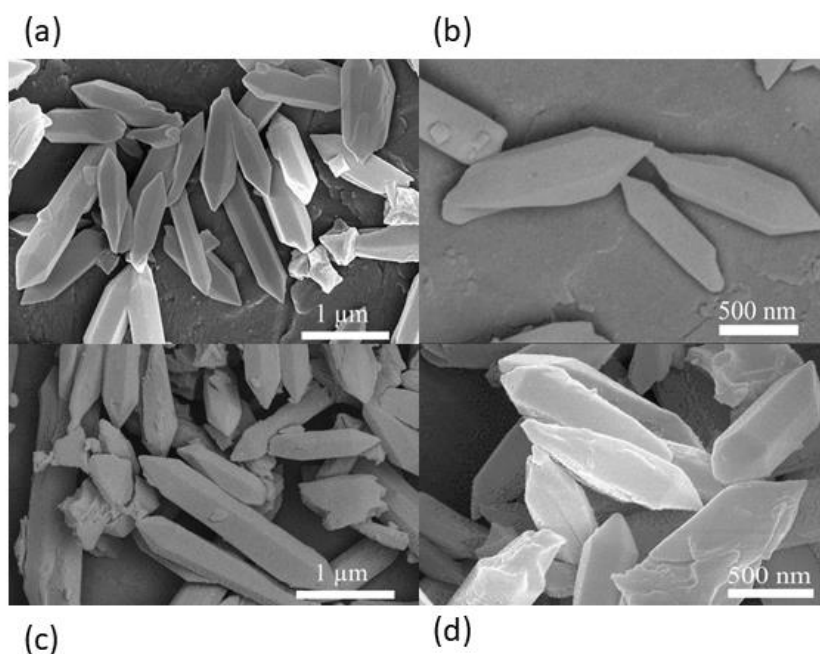
Figure 23: FE-SEM for NH_2-MIL88(Fe) MOF. (a) at 1 µm for fresh sample, (b) at 500 nm for fresh sample, (c) at 1 µm for mercury adsorbed sample and (d) at 500 nm for mercury adsorbed sample.

The FE-SEM images of NH_2-MIL53(Al) MOF, displayed in Figure 24, exhibit a clustered nodular structure with single globular grains [50]. Figures 24 (a), (b) and (c) show a fresh sample of the MOF, while Figures 24 (d), (e) and (f) show the MOF sample after mercury adsorption. The grain feature is comparable to that observed by Zhang et al. [50], where the MOF evidently retains its structure and morphological characteristics after mercury uptake.
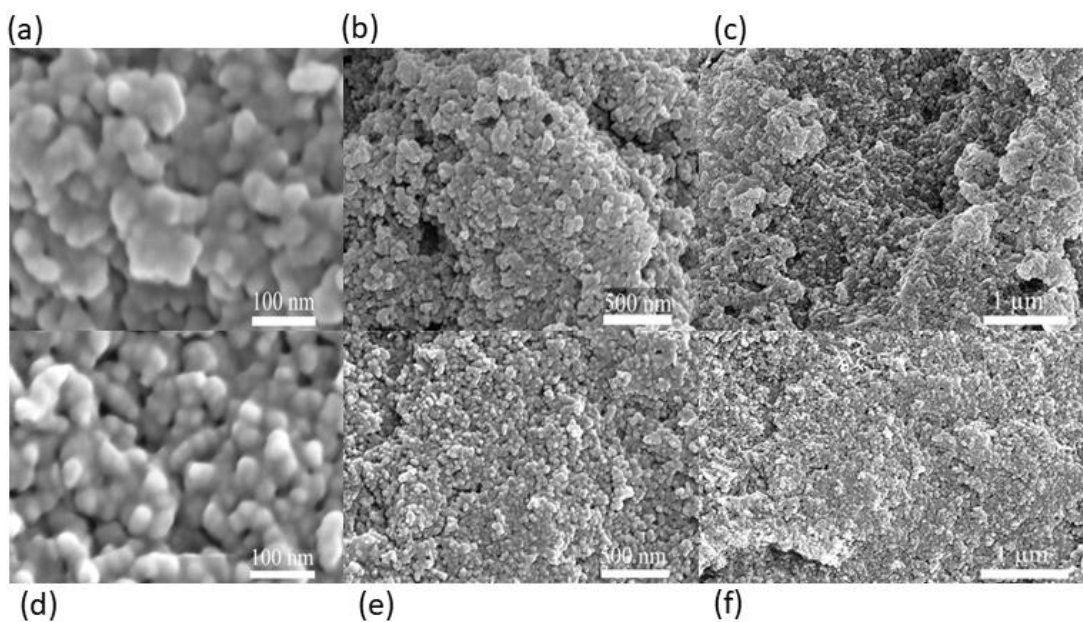
Figure 24: FE-SEM for NH$_2$-MIL53(Al) MOF. (a) at 100 nm fresh sample, (b) at 500 nm for fresh sample, (c) 1 µm for fresh sample (d) at 100 nm for mercury adsorbed sample, (e) at 500 nm for mercury adsorbed sample and (f) at 1 µm for mercury adsorbed sample.
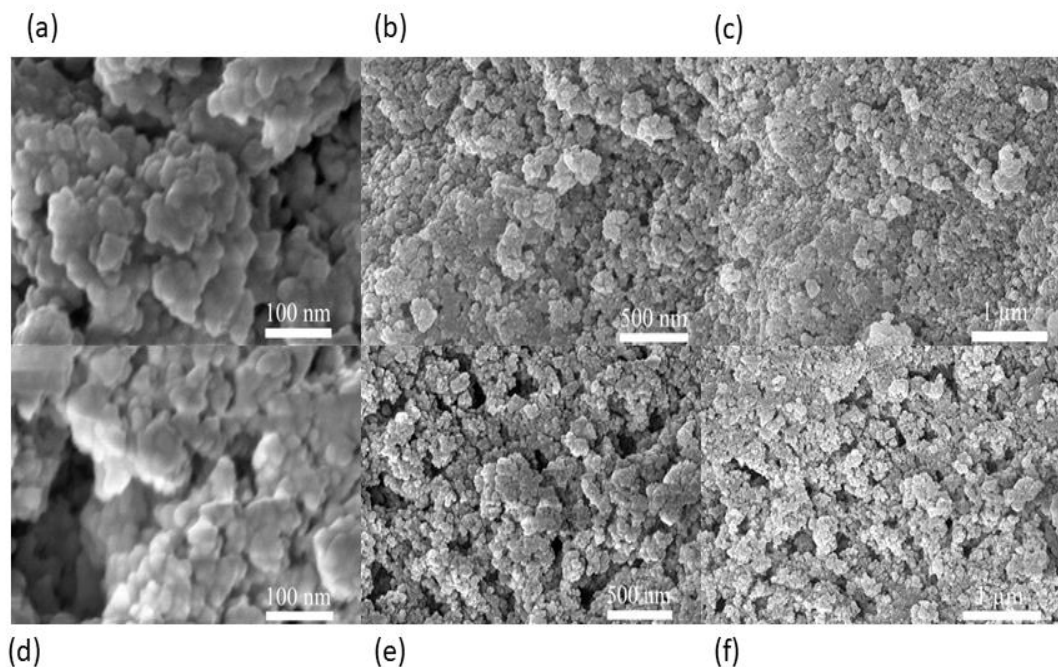
Figure 25: FE-SEM for NH$_2$-UiO-66(Zr) MOF. (a) at 100 nm fresh sample, (b) at 500 nm for fresh sample, (c) 1 µm for fresh sample (d) at 100 nm for mercury adsorbed sample, (e) at 500 nm for mercury adsorbed sample and (f) at 1 µm for mercury adsorbed sample.

The FE-SEM images of NH_2-UiO-66(Zr) are shown in Figure 25. They show an hexagon and amorphous structure, which confirm the findings from XRD and the FTIR results as well as being supported by previous works in the literature [104]. Figures 25 (a), (b) and (c) show a fresh sample of the MOF, while Figures 25 (d), (e) and (f). Mercury uptake seems to have damaged the structure more severely than its Al-MOF counterpart, possibly due to the randomness of the structure with numerous dangling bonds that allow the intercalation of Hg material.

4.2.1.4 TGA. The results of TGA analysis conducted on all MOFs under investigation are shown in Figure 26. A good agreement with the results reported in previous works cited in the literature [50], [104]–[106] is obtained. For example, the current TGA results of NH_2-MIL88(Fe) were found consistent with the results reported by Kim et al. [106] and the TGA results for NH_2-MIL53(Al) and NH_2-UiO-66(Zr) MOF are consistent with those obtained by Zhang et al. [50] and Fu et al. [104], respectively. It should be noted that the NH_2-MIL88(Fe) MOF has the lowest thermal stability and its structure losses its rigidity faster than the other MOFs. A general trend is observed for all MOFs, showing a steady weight drop at ~100°C due to moisture and unreacted chemicals escaping the structure [84]. The immediate weight loss of NH_2-MIL88(Fe) MOF is due to the high moisture content which has diverse effect on its structural stability, as reported in Ma et al. [105]. Compared to the other MOFs, the Cd-MOF exhibited the highest capability of retaining its moisture after the initial drop which occur around 200 °C rather than 100 °C.

The TGA results show that the amorphous Zr-MOF remains insensitive to temperature rise compared to the other MOFs. This is mainly due to its high temperature treatment during the synthesis procedure as confirmed by Fu et al. [104]. The MOF's lack of crystallinity affects the response to the heating temperature sweep due to the highly defective and random structure [104]. For the other three MOFs, the TGA analysis shows all tested MOFs experience two major drops, indicating a complete loss of rigidity. The first peak obtained around 200°C is due to the loss of the NH_2-Cd-BDC linker undergoing an alteration and resemblance in its polymer bonds [85], [86]. This is more evident for the NH_2-Cd-BDC MOF more than NH_2-MIL88(Fe) MOF due to the higher structure stability of the latter. However, compared to the NH_2-MIL53(Al) MOF, this drop is much smaller, indicating that the alteration in polymer bonds of the

60

MOF takes place at a later stage. This is renders that the MOF is more resistant to heat at this specific temperature. Moreover, the NH$_2$-MIL88(Fe) MOF experiences the first major drop when exposed to a temperature of 250°C and then the weight decreases steadily until reaching ~450°C at which the MOF structure collapses [106]. As for the NH$_2$-Cd-BDC MOF, the first noticeable drop occurs at 200°C. The curve flattens and then undergoes a second abrupt drop to low values when reaching the temperature 400°C. The curve flattens again indicating the structure collapse of the organic linker as the polymer bonds are affected by the heating mechanism [86]. We note that for the NH$_2$-Cd-BDC MOF, the curve reaches saturation at 580°C demonstrating the complete collapse of the crystalline structure [86]. Similar to the Cd-MOF, the NH$_2$-MIL53(Al) has a high overall thermal stability as the MOFs curves experience a slightly similar weight loss pattern. However, the Al-MOF experiences it first major drop at 500°C and this shows that the Al-MOF holds its structure more firmly than the Cd-MOF at higher temperatures. Similar to the Fe-MOF, the Al-MOF weight loss percentage drops very low and experiences complete collapse at a temperature of around 550°C. The TGA results revealed that NH$_2$-Cd-BDC and NH$_2$-MIL53(Al) MOFs have a higher thermal stability in comparison to the NH$_2$-MIL88(Fe) MOF. However, given to its defects in the structure, the NH$_2$-UiO-66(Zr) MOF has a very high thermal stability, as indicated by the level of the weight loss and the variations in the slope with temperature [104].
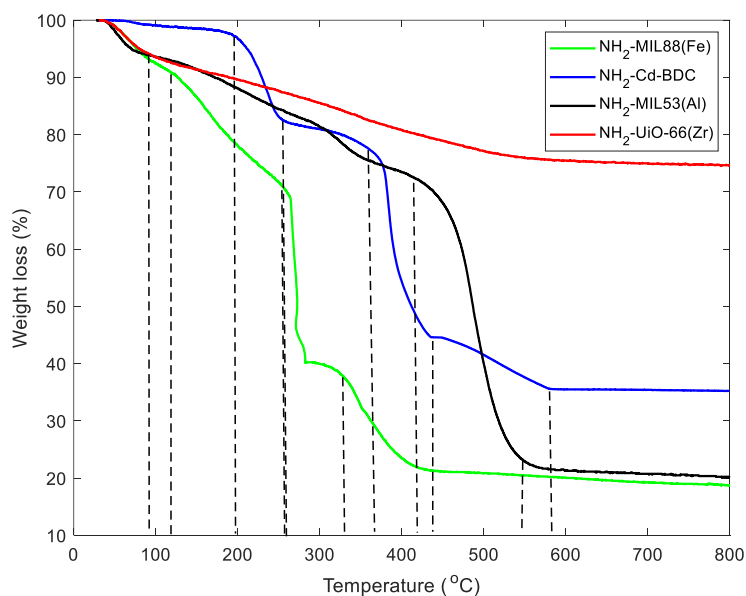
Figure 26: TGA results for the 4 MOFs. Green curve is for NH$_2$-MIL88(Fe), blue curve for NH$_2$-Cd-BDC, black curve for NH$_2$-MIL(53) and red curve for NH$_2$-UiO-66(Zr).

4.2.2. Mercury detection: A comparative analysis. The results of the comparative study will be presented in this section.

4.2.2.1 Mercury ions detection. The four MOFs have been tested for immediate mercury ions detection. The results are shown in Figure 27. Figure 27 (a) is for the NH$_2$-Cd-BDC MOF, Figure 27 (b) is for the NH$_2$-MIL53(Al) MOF, Figure 27 (c) is for the NH$_2$-MIL88(Fe) MOF and Figure 27 (d) is for the NH$_2$-UiO-66(Zr) MOF. The blue curve in all the figures indicate the baseline curve that shows the MOF intensity. Keeping the fluorometer settings same for all MOFs and using the same testing procedure, it can be noted that the NH$_2$-Cd-BDC MOF has the highest intensity. This can be attributed to the fact that Cd-MOFs have higher intensity due to the cadmium itself possessing some fluorescence ability [93]. The NH$_2$-MIL53(Al) MOF and the NH$_2$-UiO-66(Zr) MOF have shown almost similar baseline intensity. The NH$_2$-MIL88(Fe) showed the least baseline intensity.

Figure 27: Mercury detection results at a concentration of 200 µM. (a) for NH$_2$-Cd-BDC, (b) for NH$_2$-MIL53(Al), (c) for NH$_2$-MIL88(Fe) and (d) for NH$_2$-UiO-66(Zr).

The orange curve in the figures represents the MOFs intensity after mercury detection. All the MOFs were exposed to a mercury concentration of 200 µM. All MOFs showed an immediate and fast response to mercury ions. Based upon the calculation method used in Chapter 3, the NH_2-Cd-BDC MOF experienced the highest quenching percentage of 93 % followed by NH_2-MIL53(Al) with 92.7 %. The NH_2-MIL88(Fe) experienced a quenching percentage of 89% and the NH_2-UiO-66(Zr) experienced a quenching percentage of 79%. These results are consistent with what was reported by Zhang et al. [50] for the Al, Fe and Zr MOFs. This shows that the Cd-MOF has the superiority in detection. Also, all the MOFs were anticipated to be able to detect mercury ions efficiently due to the presence of the NH_2 functionalized group. As discussed in Chapter 3, the amino-functionalized group is a nucleophilic center that causes an attractive point for mercury ions to bind in. The binding causes a change in the structure; thus, the quenching happens as the fluorescence of the MOF gets affected [50], [51], [107]. However, the percentage difference in the quenching is mostly attributed to the orientation of the MOF and the accessibility of the NH_2 molecule [50].

4.2.2.2 Single ion competition. To investigate the mercury selectivity of all four MOFs, several experiments were conducted on different metal ions that may co-exist with mercury in an aqueous environment. Aqueous solutions of a concentration of 1000 µM were prepared for 6 different metal ions, namely: Pb^{3+}, Cr^{3+}, Fe^{3+}, K^+, Na^+ and Ca^{2+}, Cd^{2+}, Cu^{2+} and Hg^{2+} ions. The MOFs were suspended in each aqueous solution and instantaneous measurements of the quenching were taken. We note that the final concentration that the MOF was detecting due to dilution effect is 200 µM. The quenching percentage calculations were performed as described in Chapter 3. Figure 28 and Figure 29 show the results of the single ion test for the four MOFs under investigation. Figure 28 represent a histogram showing the detection percentage of each MOF for each ion at the concentration of 200 µM. We display in Figure 29 the 3D plots of the intensity of the four MOFs when exposed to different ions to enable better visualization of the single ion detection results. All four MOFs show high selectivity towards mercury compared to the other metal ions. Furthermore, all four MOFs are observed to be insensitive to the sodium, potassium and calcium ions [54]. For the cadmium ions, only the NH_2-MIL88(Fe) MOF show a slight response. Investigating the MOFs behavior towards the chromium ions, we can observe that all the MOFs show similar behavior. A detecting percentage of about 60% is obtained for the NH_2-

MIL88(Fe) and NH2-Cd-BDC. On the other hand, about 50% is obtained for the NH2-MIL53(Al) and NH2-UiO-66(Zr) MOF. As for the lead ions, the NH2-MIL53(Al) and NH2-UiO-66(Zr) MOFs show a detecting percentage of about 70%, while the NH2-MIL88(Fe) had a detectingg percentage close to 75%. However, the NH2-Cd-BDC presented the most detecting capability due to lead ions with a detecting percentage close to 85%. Again, this is comparable to what was reported in literature [50], [54].
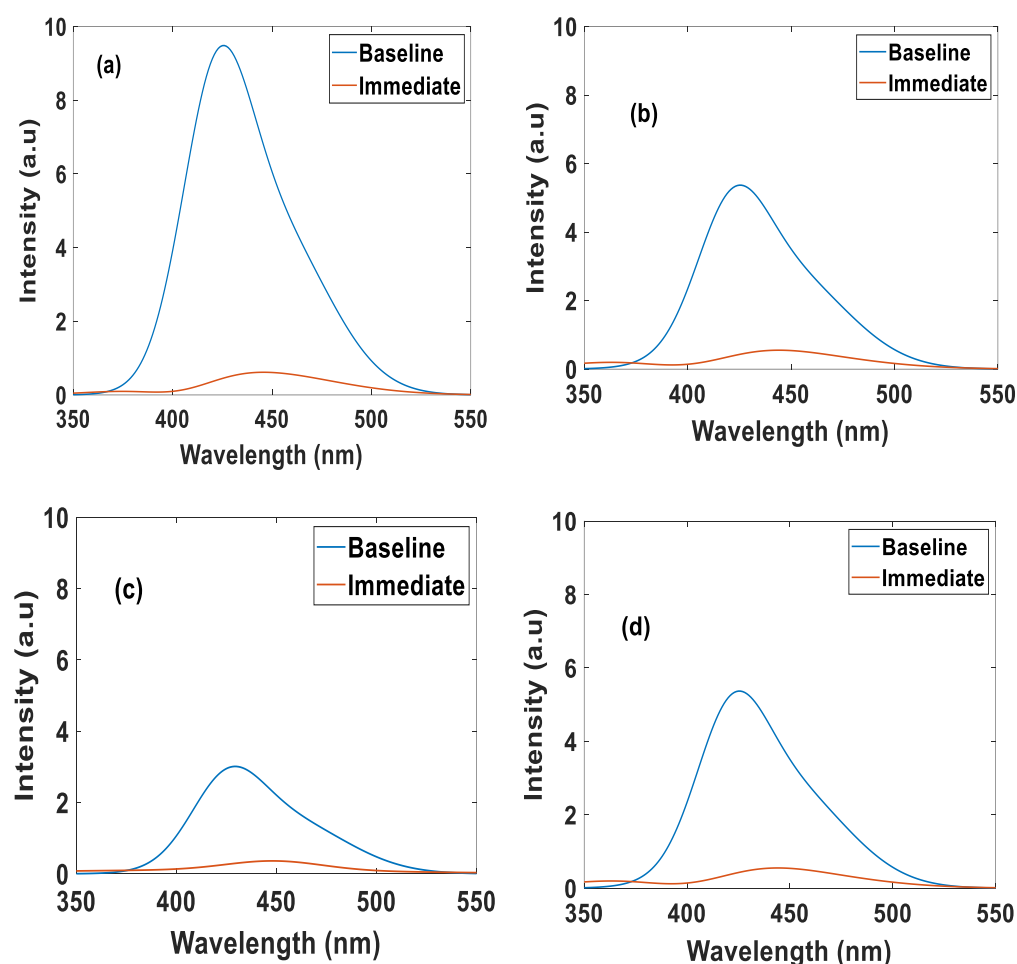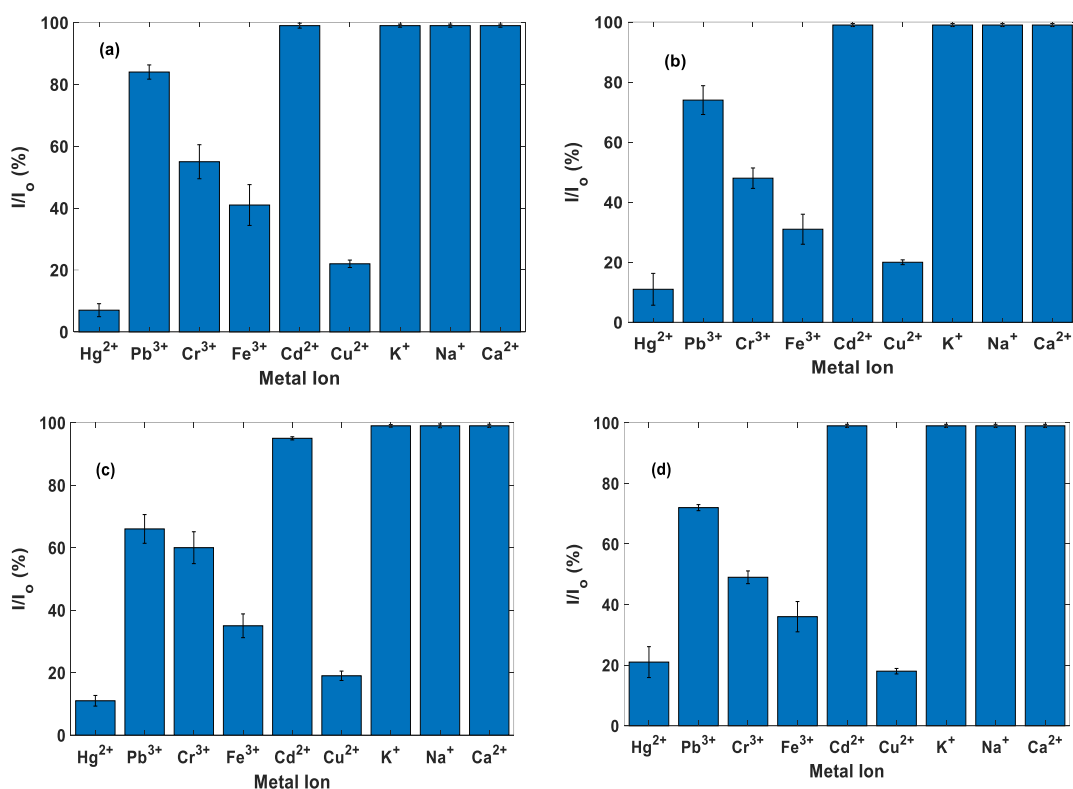

Figure 28: Single ion detection results at a concentration of 200 µM. (a) for NH2-Cd-BDC, (b) for NH2-MIL53(Al), (c) for NH2-MIL88(Fe) and (d) for NH2-UiO-66(Zr).

The most competitive ions to mercury in terms of selectivity are iron and copper ions. For the iron ions, the NH2-Cd-BDC MOF show a detecting percentage of around 43%, which is the highest amongst all the other MOFs. The other MOFs all experienced a detecting percentage around 30%. This shows a slight superiority of the Cd-MOF compared to the other MOFs. Inspecting the behavior of the MOFs when exposed to the copper ions, we observe that all MOFs exhibit a noticeable detecting percentage that can be approximated around 20%. This is in agreement with some findings reported in the literature on copper ions interaction [54], [97], [101]. This is due to the fact that

the copper ions have similar properties to those of the mercury ions as they both belong to the same group of transition metals in the periodic table.

All the single ion experiments were repeated three time to ensure that the results obtained are repeatable and reproducible. The standard deviation values are shown by the error bars on the histograms of Figure 28. The maximum standard deviation was found equal to 10%. This indicates the repeatability of the experiments.
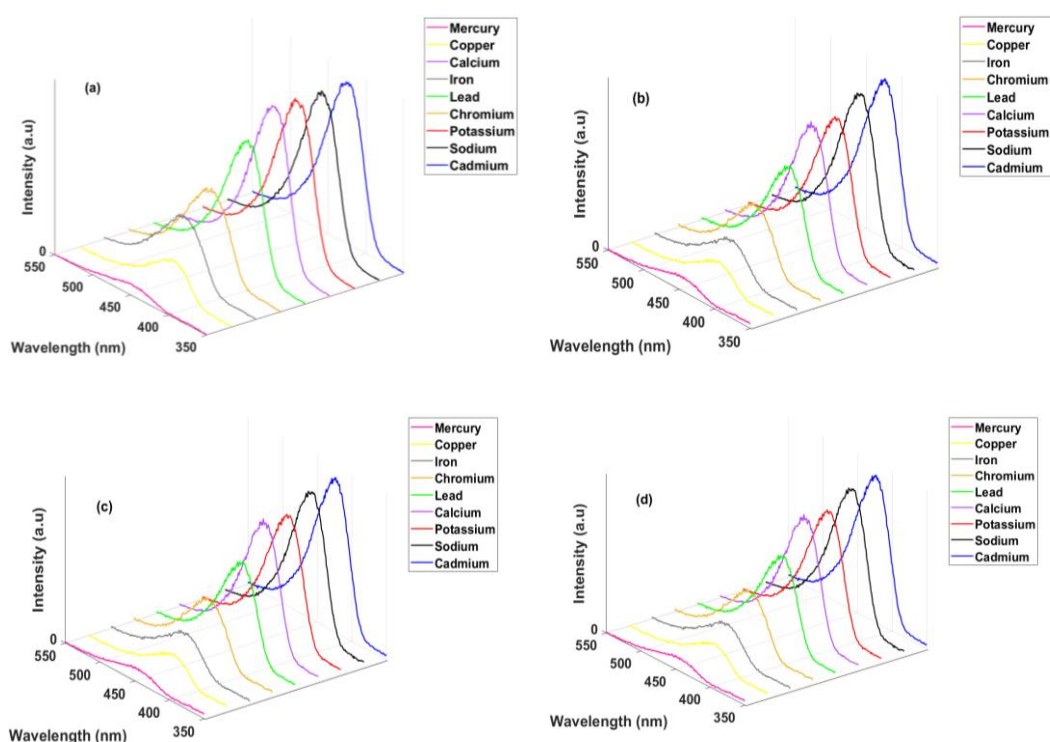
Figure 29: Single ion 3D detection results at a concentration of 200 µM. (a) for NH2-Cd-BDC, (b) for NH2-MIL53(Al), (c) for NH2-MIL88(Fe) and (d) for NH2-UiO-66(Zr).

4.2.2.3 Limit of detection. An important performance metric to investigate the capability of the MOF to detect mercury is the limit of detection (LOD). As such, the LOD of the four MOFs were identified using a similar testing technique as performed for the single ion test. To do so, the concentration of the mercury was incrementally reduced from 200 µM to a level where no further quenching is observed. Figure 30 shows the variations of the fluorescence intensity with the wavelength for the different mercury concentrations. The results are shown for all MOFs. The graphs show that the Cd, Al and Zr MOFs have all reached to a concentration of 2 µM, while the Fe-MOF

stopped detecting mercury at a concentration of 4 µM. However, further analysis of the limit of detection is carried out following the Stern Volmer calculation procedure, which is described in details in Chapter 3. Figure 31 show the graphical results found from applying the Stern Volmer procedure. In this calculation, the lowest concentrations with the highest linear best fit are chosen to predict the limit of detection value. Upon performing that, the slope and intercept from the Stern Volmer graphs are used to calculate the LOD. The calculated LOD values were 0.58 µM for NH_2-Cd-BDC MOF, 0.51 µM for NH_2-MIL53 (Al) MOF, 1.03 µM for NH_2-MIL88(Fe) MOF and 1.94 µM for NH_2-UiO-66(Zr) MOF.
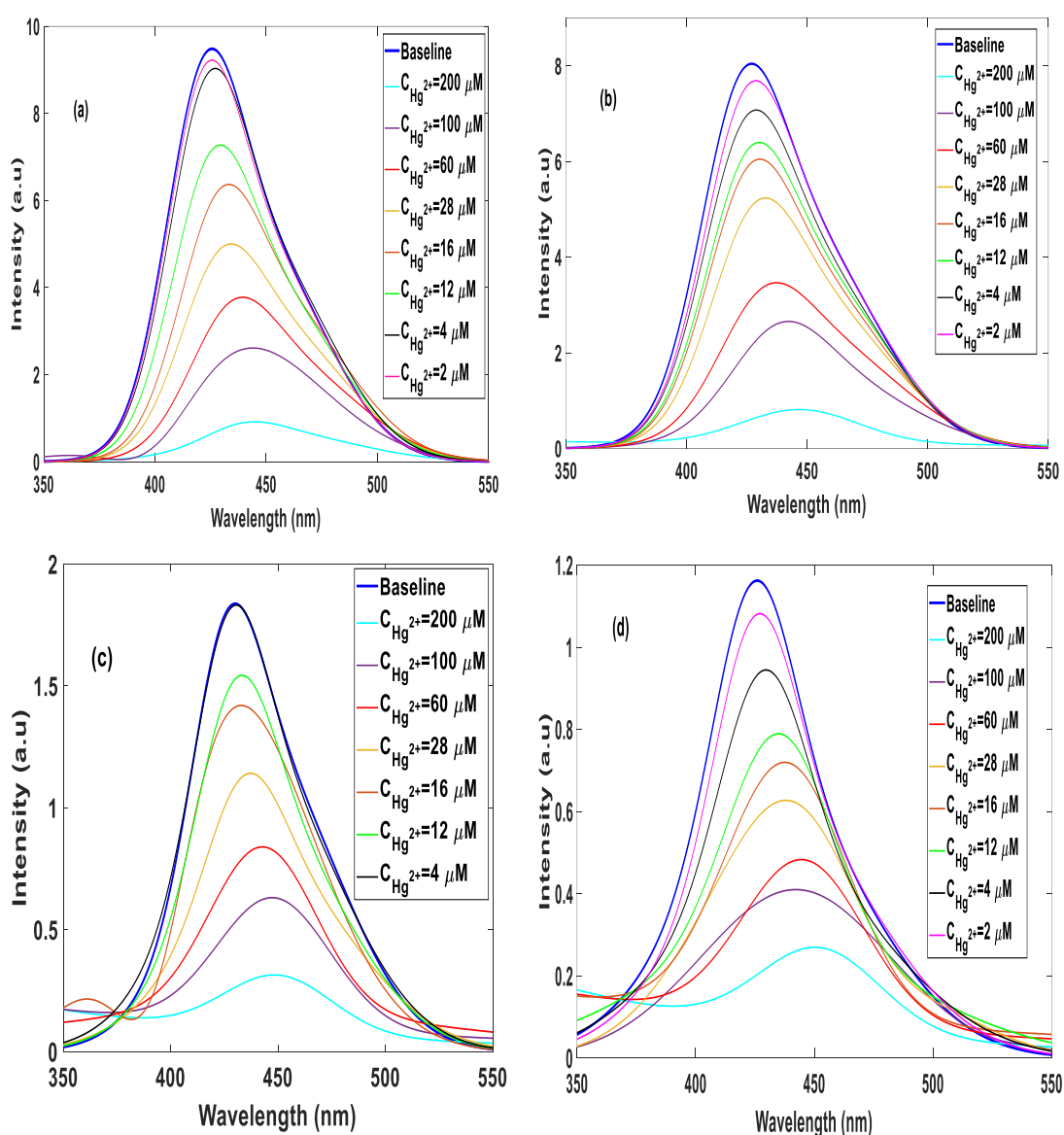
Figure 30: Different concentration detection results. (a) for NH_2-Cd-BDC, (b) for NH_2-MIL53(Al), (c) for NH_2-MIL88(Fe) and (d) for NH_2-UiO-66(Zr).

66
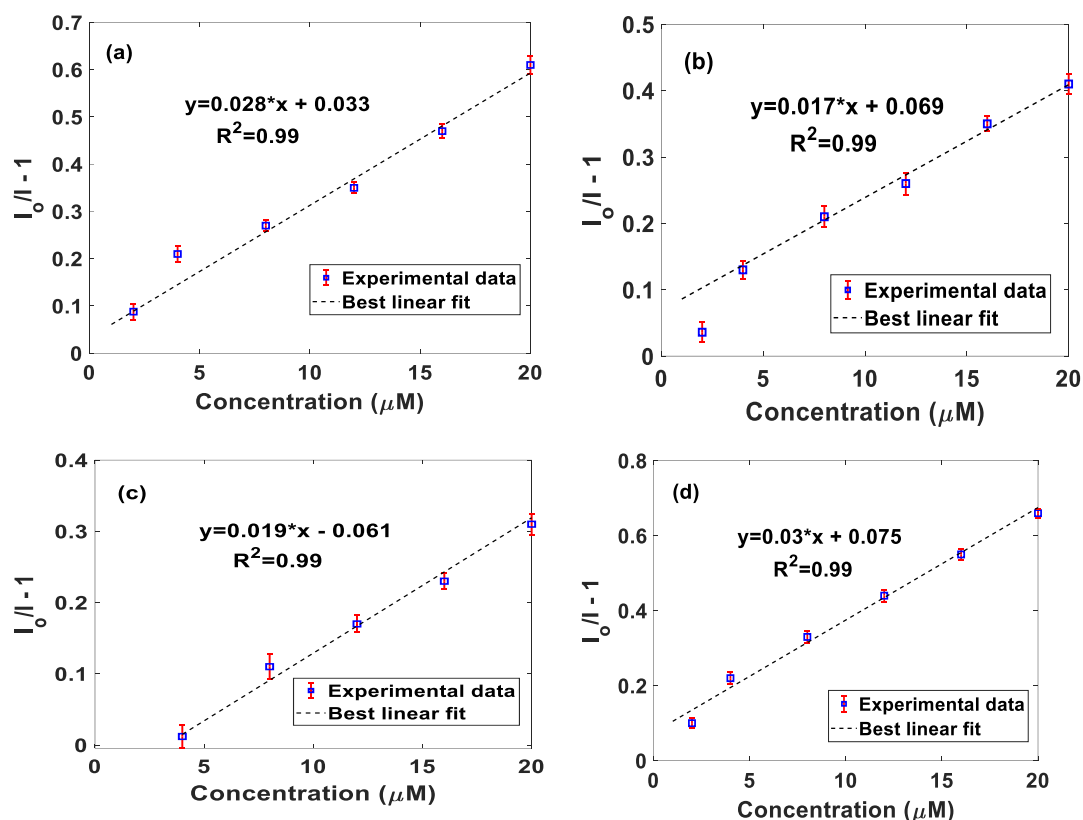
Figure 31: Limit of detection results using Stern-Volmer method. (a) for NH_2-Cd-BDC, (b) for NH_2-MIL53(Al), (c) for NH_2-MIL88(Fe) and (d) for NH_2-UiO-66(Zr).

Comparing the values of the LOD obtained above, a slight superiority in the LOD can be seen for the NH_2-MIL53(Al) MOF. This is consistent with what is reported in the literature on Al-MOFs being superior detectors of mercury ions as they have the best coordination that allows for easier access of the mercury ions and allows for efficient detection [50], [87]. We note that the value of the LOD for the NH_2-MIL53(Al) is different from the one reported by Zhang et al. [50]. This could be attributed to the difference in the synthesis procedure. The present microwave-assisted synthesis may have resulted in some slight structural changes that led to higher LOD values. Moreover, the equipment limitation can be one of the possible reasons for the difference in the LOD values. As for the NH_2-MIL88(Fe) and NH_2-UiO-66(Zr) MOFs, there lower limit of detection is consistent with the conclusions made by Zhang et al. [50]. The NH_2-Cd-BDC MOF showed a good LOD and very comparable to the Al-MOF, which indicates the high potential of the MOF as a mercury detector.

All the LOD experiments were repeated three time to ensure that the results obtained are repeatable and reproducible. The standard deviation values are shown by the error bars on the histograms of Figure 31. The maximum standard deviation was found equal to 14%. This indicates the repeatability of the experiments.

4.2.2.4 Competitive environment detection. Competition between ions in aqueous solution is of great importance when investigating the MOFs detection capability. To verify the MOFs selectivity, a solution of the ions Pb^{3+}, Cr^{3+}, Fe^{3+}, K^+, Na^+, Ca^{2+}, Cd^{2+} and Cu^{2+} was prepared with a concentration of 2000 µM while adding a solution containing Hg^{2+} ions with a concentration of 1000 µM. The actual concentrations upon dilution with the MOF solution during the test is 400 µM for the metal ions and 200 µM for the mercury. The reading of the photoluminescence quenching was taken before and after the addition of mercury ions. The photoluminescence detection readings are shown in Figure 32. The experimental results of the competition test reveal that the NH_2-Cd-BDC has a higher selectivity for mercury ions when compared to the other MOFs. Interestingly, the NH_2-UiO-66(Zr) MOF has the second highest selectivity for mercury ions in the competitive environment. This could be attributed to the fact that the Zr-MOF has less affinity to the other chemical ions when they are at high concentrations [50]. The NH_2-MIL53(Al) MOF and the NH_2-MIL88(Fe) MOF showed lower performance in the double concentration test.
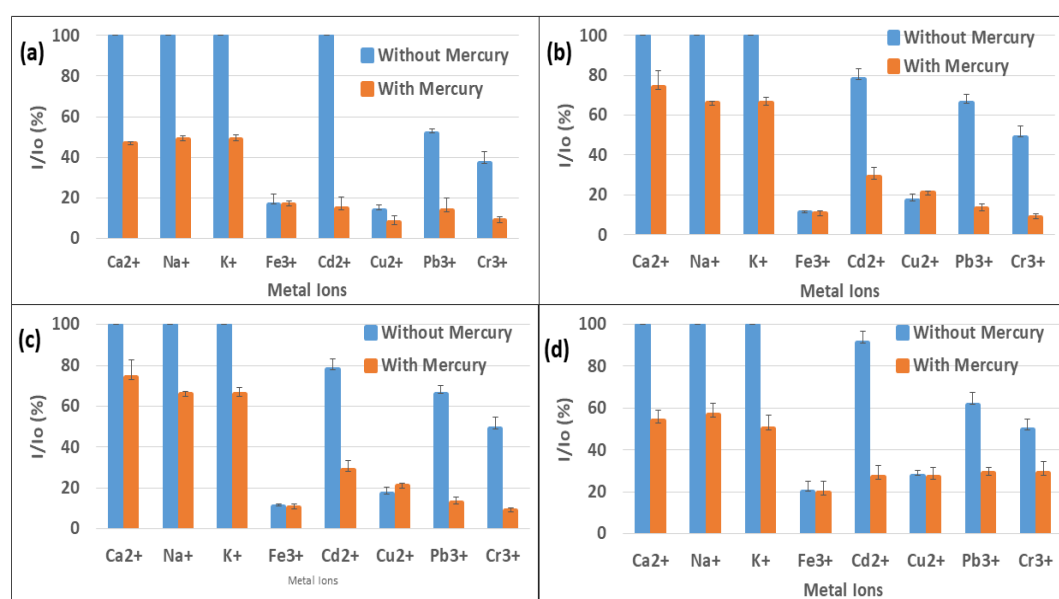
Figure 32: Competitive environment results. (a) for NH_2-Cd-BDC, (b) for NH_2-MIL53(Al), (c) for NH_2-MIL88(Fe) and (d) for NH_2-UiO-66(Zr).

68

Inspecting the performance of the MOFs when it comes to individual ions. All MOFs showed no response to K^+, Na^+ and Ca^{2+} ions even when doubling their concentration. For the Cd^{2+}, the NH₂-Cd-BDC MOF did not show any detection but the other MOFs showed some slight detection. This is consistent with what is stated in literature about MOFs being unresponsive to detecting metal ions that they are composed of [51]. For Pb^{3+} ions, all the MOFs showed detection of the ion with slight variations in the detection percentage. However, when the mercury ions was added, all the MOFs showed further quenching indicating the ability to detect mercury still. NH₂-UiO-66(Zr) MOF showed the least detection of mercury. For Cr^{3+} ions, the NH₂-Cd-BDC showed more sensitivity when the concentration is doubled compared to all the other MOFs. Similar to the Pb^{3+} ions behavior, all the MOFs further quenched after mercury addition and the NH₂-UiO-66(Zr) MOF showed the least detection of mercury.

For the Fe^{3+} ions, all the MOFs showed high detection abilities for the 2000 µM concentration. NH₂-MIL88(Fe) and NH₂-Cd-BDC MOFs showed the highest detection. However, all the MOFs showed further detection when the mercury was added to the solution. Even though the percentage change is small, the detection of mercury can be observed by noticing a shift in the peak. This shift in the peak is an indication of the mercury altering the structure of the MOF. This is consistent with what was reported in literature by Liu et al. [51]. For the Cu^{2+} ions, the scenario is a bit different. All MOFs detected copper ions at the high concentration. NH₂-UiO-66(Zr) was the least responsive to the copper ions while the other MOFs had similar detection response. However, the NH₂-Cd-BDC MOF showed the highest difference between before and after mercury addition. This indicates its superior selectivity. Moreover, the NH₂-MIL88(Fe) and NH₂-MIL53(Al) also have a superior selectivity due to the increase in the percentage of detection after mercury addition. This happens due to the fact that when the mercury is added, it substitutes some of the already attached copper on the MOF structure. This causes the copper ions to get released again to the solution. This phenomena causes the fluorescence intensity to increase as the copper ions are fluorescent themselves. This is consistent with what was reported by Zhang et al. [54], where the copper ions were seen to increase the intensity of the fluorescence when they were not absorbed by the MOF that was produced. The NH₂-UiO-66(Zr) showed the least response after adding the mercury ions. It can be concluded from these results that the NH₂-MIL53(Al) and the NH₂-Cd-BDC MOFs are superior in terms of the

competitive environment analysis due to their high response to mercury and least response to other metal ions.

All the competitive ion experiments were repeated three time to ensure that the results obtained are repeatable and reproducible. The standard deviation values are shown by the error bars on the histograms of Figure 32. The maximum standard deviation was found equal to 13%. This indicates the repeatability of the experiments.

4.3. Conclusion

In this chapter, the capability of four MOFs, namely NH_2-Cd-BDC, NH_2-MIL88(Fe), NH2-MIL53(Al) and NH2-UiO-66(Zr) to detect mercury in competitive environment was inspected. These MOFs comprise the same organic linker 2-aminoterephthalic acid but different metal clusters (cadmium, aluminum, zirconium and iron). All MOFs were successfully synthesized using microwave irradiation, being a fast and ecofriendly technique to produce MOFs while preserving their crystalline structure. The synthesized MOFs were characterized by performing XRD, FTIR, TGA and FE-SEM tests. A series of experiments using fluorometric analysis was conducted to assess the performance of the MOFs in terms of fast and selective detection of mercury. The characterization tests confirmed that all the MOFs maintained their crystalline structures except for the NH2-UiO-66(Zr) due to the amorphous structure of the as-synthesized sample. Also, it was concluded that the NH_2-Cd-BDC MOF and the NH2-MIL53(Al) MOFs are superior to the NH_2-MIL88(Fe) and NH2-UiO-66(Zr) MOFs in terms of mercury detection and selectivity in a competitive environment as manifested by the higher quenching levels of the fluorescence intensity. The limit of detection was found equal to 0.58 µM, 0.51 µM, 1.03 µM and 1.94 µM for the NH_2-Cd-BDC, NH_2-MIL53(Al), NH_2-MIL88(Fe) and NH_2-UiO-66(Zr), respectively.

Chapter 5. Conclusion and Future Work

The present thesis deals with the development, characterization and analysis of Metal Organic Frameworks (MOFs) that can detect mercury in aqueous environments at low concentrations. A novel MOF, namely NH_2-Cd-BDC was synthesized using microwave-assisted synthesis procedure, being a fast and low-energy synthesis route. This MOF showed superb detection abilities for mercury in competitive environments. Its performance was also compared to three other MOFs comprising the same organic linker and different metal clusters (aluminium, zirconium and iron). All the MOFs were characterized and their performance for mercury detection in the presence of other heavy metal ions was studied. Given the reported superb capabilities of the NH_2-MIL53(Al) MOF for mercury detection, the NH_2-Cd-BDC showed competitive performance indicating the success of synthesizing a candidate competitor MOF. The LOD values obtained from the experiments were 0.58 µM for NH_2-Cd-BDC MOF, 0.51 µM for NH_2-MIL53 (Al) MOF, 1.03 µM for NH_2-MIL88(Fe) MOF and 1.94 µM for NH_2-UiO-66(Zr) MOF. Furthermore, all the MOFs showed similar behavior when exposed to mercury in presence of other metal ions, as they all showed the greatest detection towards mercury ions. The NH_2-MIL53(Al) superiority was confirmed through the lowest LOD and high detection capability of mercury ions. Of interest, the NH_2-Cd-BDC MOF showed very comparable performance to that of the NH_2-MIL53(Al) as their LOD values were very close to each other. Similarly, the mercury detection ion tests further confirmed how comparable the behavior of the two MOFs are. The present experiments revealed that the NH_2-MIL88(Fe) and NH_2-UiO-66(Zr) MOFs have lower performance, which similar to the results reported in the literature.

Future works on the novel MOF can include the study of the MOF performance as a dual material for simultaneous detection and capturing mercury from aqueous solutions. This constitutes a promising research line. Furthermore, the developed MOF has the potential to be integrated with the MEMS technology to develop a fully functional chemical sensor for detecting mercury in aqueous solutions. The MOF can be deposited on a micro-beam using adhering material and sophisticated localized deposition techniques. This allows for the development of a chemical sensor that can be remotely operated and is capable of detecting low levels of mercury. Finally,

investigating the performance of the developed MOF/composite and the integrated fully functional chemical sensor can be performed utilizing real matrix seawater samples.

References

[1]   T. Mahoney, *Mercury*. New YorK: Springer, 2014.

[2]   L. Froboese, P. Titscher, B. Westphal, W. Haselrieder, and A. Kwade, "Mercury intrusion for ion- and conversion-based battery electrodes – Structure and diffusion coefficient determination," *Mater. Charact.*, vol. 133, pp. 102–111, Nov. 2017.

[3]   A. Guo, M. Durymanov, A. Permyakova, S. Sene, C. Serre, and J. Reineke, "Metal Organic Framework (MOF) Particles as Potential Bacteria-Mimicking Delivery Systems for Infectious Diseases: Characterization and Cellular Internalization in Alveolar Macrophages," *Pharm. Res.*, vol. 36, no. 4, pp. 1–11, Apr. 2019.

[4]   T. Ghanbari, F. Abnisa, and W. M. A. Wan Daud, "A review on production of metal organic frameworks (MOF) for CO2 adsorption," *Science of the Total Environment*, vol. 707. p. 135090, 10-Mar-2020.

[5]   R. F. Mendes, J. Rocha, and F. A. Almeida Paz, "Microwave synthesis of metal-organic frameworks," in *Metal-Organic Frameworks for Biomedical Applications*, vol. 55. pp. 159–176.

[6]   K. H. Vardhan, P. S. Kumar, and R. C. Panda, "A review on heavy metal pollution, toxicity and remedial measures: Current trends and future perspectives," *Journal of Molecular Liquids*, vol. 290. p. 111-197, 15-Sep-2019.

[7]   H. Qin, T. Hu, Y. Zhai, N. Lu, and J. Aliyeva, "The improved methods of heavy metals removal by biosorbents: A review," *Environmental Pollution*, vol. 258. p. 113777, 01-Mar-2020.

[8]   L. Joseph, B. M. Jun, J. R. V. Flora, C. M. Park, and Y. Yoon, "Removal of heavy metals from water sources in the developing world using low-cost materials: A review," *Chemosphere*, vol. 229. pp. 142–159, 01-Aug-2019.

[9]   S. Z. N. Ahmad, W. N. Wan Salleh, A. F. Ismail, N. Yusof, M. Z. Mohd Yusop, and F. Aziz, "Adsorptive removal of heavy metal ions using graphene-based nanomaterials: Toxicity, roles of functional groups and mechanisms," *Chemosphere*, vol. 248. p. 126008, 01-Jun-2020.

[10]   H. Alidadi, S. B. Tavakoly Sany, B. Zarif Garaati Oftadeh, T. Mohamad, H. Shamszade, and M. Fakhari, "Health risk assessments of arsenic and toxic heavy metal exposure in drinking water in northeast Iran," *Environ. Health Prev. Med.*, vol. 24, no. 1, p. 59, Sep. 2019.

[11]   P. B. Tchounwou, C. G. Yedjou, A. K. Patlolla, and D. J. Sutton, "Heavy metal toxicity and the environment," *EXS*, vol. 101, pp. 133–164, 2012.

[12]   A. L. Wani, A. Ara, and J. A. Usmani, "Lead toxicity: A review," *Interdisciplinary Toxicology*, vol. 8, no. 2. pp. 55–64, 01-Jun-2015.

[13]   A. C. Bittarello, J. C. S. Vieira, C. P. Braga, and I. da Cunha Bataglioli, "Metalloproteomic approach of mercury-binding proteins in liver and kidney

tissues of Plagioscion squamosissimus (corvina) and Colossoma macropomum (tambaqui) from Amazon region: Possible identification of mercury contamination biomarkers," *Sci. Total Environ.*, vol. 711, p. 134547, Apr. 2020.

[14] "Mercury and health," 31-Mar-2017. [Online]. Available: https://www.who.int/news-room/fact-sheets/detail/mercury-and-health. [Accessed: 07-Nov-2020].

[15] L. Barregard, "Health effects of inorganic mercury," *Toxicol. Lett.*, vol. 164, p. S11, Sep. 2006.

[16] R. Miniero, E. Beccaloni, M. R. Cicero, R. Scenati, and D. Lucchetti, "Mercury (Hg) and methyl mercury (MeHg) concentrations in fish from the coastal lagoon of Orbetello, central Italy," *Mar. Pollut. Bull.*, vol. 76, no. 1–2, pp. 365–369, Nov. 2013.

[17] L. Yang, Y. Zhang, F. Wang, Z. Luo, S. Guo, and U. Strähle, "Toxicity of mercury: Molecular evidence," *Chemosphere*, vol. 245. Elsevier Ltd, p. 125586, 01-Apr-2020.

[18] O. Linhart, A. Kolorosová-Mrázová, J. Kratzer, J. Hraníček, and V. Červený, "Mercury Speciation in Fish by High-Performance Liquid Chromatography (HPLC) and Post-Column Ultraviolet (UV)-Photochemical Vapor Generation (PVG): Comparison of Conventional Line-Source and High-Resolution Continuum Source (HR-CS) Atomic Absorption Spectrometry (AAS)," *Anal. Lett.*, vol. 52, no. 4, pp. 613–632, Mar. 2019.

[19] M. Guo, J. Wang, R. Du, Y. Liu, and J. Chi, "A test strip platform based on a whole-cell microbial biosensor for simultaneous on-site detection of total inorganic mercury pollutants in cosmetics without the need for predigestion," *Biosens. Bioelectron.*, vol. 150, pp.78-104, Feb. 2020.

[20] S. Kumari, Amit, R. Jamwal, N. Mishra, and D. K. Singh, "Recent developments in environmental mercury bioremediation and its toxicity: A review," *Environmental Nanotechnology, Monitoring and Management*, vol. 13. p. 100283, 01-May-2020.

[21] V. P. Prakashan, G. George, M. S. Sanu, P. R. Biju, and C. Joseph, "Investigations on SPR induced Cu@Ag core shell doped SiO2-TiO2-ZrO2 fiber optic sensor for mercury detection," *Appl. Surf. Sci.*, vol. 507, p. 144957, Mar. 2020.

[22] C. Wu, J. Wang, J. Shen, C. Bi, and H. Zhou, "Coumarin-based Hg2+ fluorescent probe: Synthesis and turn-on fluorescence detection in neat aqueous solution," *Sensors Actuators, B Chem.*, vol. 243, pp. 678–683, May 2017.

[23] P. J. Vikesland, "Nanosensors for water quality monitoring," *Nat. Nanotechnol.*, vol. 13, no. 8, pp. 651–660, Aug. 2018.

[24] W. Zhang, S. Li, X. Liu, Q. Zhang, and Y. Suo, "Oxygen-Generating MnO 2 Nanodots-Anchored Versatile Nanoplatform for Combined Chemo-Photodynamic Therapy in Hypoxic Cancer," *Adv. Funct. Mater.*, vol. 28, no. 13, p. 1706375, Mar. 2018.

[25]   X. Liu, L. Huang, Y. Wang, W. Zhang, and J. Wang, "One-pot bottom-up fabrication of a 2D/2D heterojuncted nanozyme towards optimized peroxidase-like activity for sulfide ions sensing," *Sensors Actuators, B Chem.*, vol. 306, p. 127565, Mar. 2020.

[26]   S. Shi, W. Zhang, H. Wu, Y. Li, and J. Liu, "In Situ Cascade Derivation toward a Hierarchical Layered Double Hydroxide Magnetic Absorbent for High-Performance Protein Separation," *ACS Sustain. Chem. Eng.*, vol. 8, no. 12, pp. 4966–4974, Mar. 2020.

[27]   C. Li, F. Zhang, X. Li, G. Zhang, and Y. Yang, "A luminescent Ln-MOF thin film for highly selective detection of nitroimidazoles in aqueous solutions based on inner filter effect," *J. Lumin.*, vol. 205, pp. 23–29, Jan. 2019.

[28]   Q. Zhang, M. Lei, J. Zhang, and Y. Shi, "A luminescent 3D Zn(II)-organic framework showing fast, selective and reversible detection of p-nitrophenol in aqueous media," *J. Lumin.*, vol. 180, pp. 287–291, Dec. 2016.

[29]   N. Jaber, S. Ilyas, O. Shekhah, M. Eddaoudi, and M. I. Younis, "Multimode excitation of a metal organics frameworks coated microbeam for smart gas sensing and actuation," *Sensors Actuators, A Phys.*, vol. 283, pp. 254–262, Nov. 2018.

[30]   X. Ma, Y. Bian, Y. Zhou, Q. Zhao, and Y. Tian, "Synthesis, Characterization, and Catalytic Property of a Hybrid Nanoscale Polyoxoniobate," *J. Clust. Sci.*, pp. 1–8, Jun. 2020.

[31]   A. Karami, R. Sabouni, and M. Ghommem, "Experimental investigation of competitive co-adsorption of naproxen and diclofenac from water by an aluminum-based metal-organic framework," *J. Mol. Liq.*, vol. 305, p. 112808, Mar. 2020.

[32]   R. Zhang, Y. Liu, Y. An, P. Wang, X. Qin, and X. Zhang, "A water-stable triazine-based metal-organic framework as an efficient adsorbent of Pb(II) ions," *Colloids Surfaces A Physicochem. Eng. Asp.*, vol. 560, pp. 315–322, Jan. 2019.

[33]   Q. Deng and R. Wang, "Heterogeneous MOF catalysts for the synthesis of trans-4,5-diaminocyclopent-2-enones from furfural and secondary amines," *Catal. Commun.*, vol. 120, pp. 11–16, Feb. 2019.

[34]   M. Ibrahim, R. Sabouni, and G. A. Husseini, "Anti-cancer Drug Delivery Using Metal Organic Frameworks (MOFs).," *Curr. Med. Chem.*, vol. 24, no. 2, pp. 193–214, 2017.

[35]   R. Sabouni and H. G. Gomaa, "Effect of hydrodynamics on nanoparticles stability in Pickering emulsions stabilized by metal organic frameworks (MOFs) in reversing shear flow," *Colloids Surfaces A Physicochem. Eng. Asp.*, vol. 484, pp. 416–423, Nov. 2015.

[36]   F. Ambroz, T. J. Macdonald, V. Martis, and I. P. Parkin, "Evaluation of the BET Theory for the Characterization of Meso and Microporous MOFs," *Small Methods*, vol. 2, no. 11, p. 1800173, Nov. 2018.

[37]   J. Yoo, U. J. Ryu, W. Kwon, and K. M. Choi, "A multi-dye containing MOF for

the ratiometric detection and simultaneous removal of Cr2O72− in the presence of interfering ions," *Sensors Actuators, B Chem.*, vol. 283, pp. 426–433, Mar. 2019.

[38] Y. Zhou, Q. Yang, D. Zhang, N. Gan, Q. Li, and J. Cuan, "Detection and removal of antibiotic tetracycline in water with a highly stable luminescent MOF," *Sensors Actuators, B Chem.*, vol. 262, pp. 137–143, Jun. 2018.

[39] S. W. Lv, J. M. Liu, C. Y. Li, N. Zhao, Z. H. Wang, and S. Wang, "A novel and universal metal-organic frameworks sensing platform for selective detection and efficient removal of heavy metal ions," *Chem. Eng. J.*, vol. 375, p. 122111, Nov. 2019.

[40] D. Ragab, H. G. Gomaa, R. Sabouni, M. Salem, M. Ren, and J. Zhu, "Micropollutants removal from water using microfiltration membrane modified with ZIF-8 metal organic frameworks (MOFs)," *Chem. Eng. J.*, vol. 300, pp. 273–279, Sep. 2016.

[41] B. Chocarro-Ruiz, J. Pérez-Carvajal, C. Avci, and O. Calvo-Lozano, "A CO2 optical sensor based on self-assembled metal-organic framework nanoparticles," *J. Mater. Chem. A*, vol. 6, no. 27, pp. 13171–13177, Jul. 2018.

[42] X. Li, J. Zhang, W. Shen, and S. Xu, "Rapid synthesis of metal-organic frameworks MIL-53(Cr)," *Mater. Lett.*, vol. 255, p. 126519, Nov. 2019.

[43] P. Tapangpan, K. Panyarat, C. Chankaew, K. Grudpan, and A. Rujiwatra, "Terbium metal organic framework: Microwave synthesis and selective sensing of nitrite," *Inorg. Chem. Commun.*, vol. 111, p. 107627, Jan. 2020.

[44] F. Mohammadnezhad, M. Feyzi, and S. Zinadini, "A novel Ce-MOF/PES mixed matrix membrane; synthesis, characterization and antifouling evaluation," *J. Ind. Eng. Chem.*, vol. 71, pp. 99–111, Mar. 2019.

[45] D. Lv, Y. Chen, Y. Li, R. Shi, and H. Wu, "Efficient Mechanochemical Synthesis of MOF-5 for Linear Alkanes Adsorption," *J. Chem. Eng. Data*, vol. 62, no. 7, pp. 2030–2036, Jul. 2017.

[46] Z. Ma, D. Wu, X. Han, H. Wang, and L. Zhang, "Ultrasonic assisted synthesis of Zn-Ni bi-metal MOFs for interconnected Ni-N-C materials with enhanced electrochemical reduction of CO2," *J. CO2 Util.*, vol. 32, pp. 251–258, Jul. 2019.

[47] N. A. Khan and S. H. Jhung, "Synthesis of metal-organic frameworks (MOFs) with microwave or ultrasound: Rapid reaction, phase-selectivity, and size reduction," *Coordination Chemistry Reviews*, vol. 285. Elsevier, pp. 11–23, 05-Feb-2015.

[48] A. Kumar, Y. Kuang, Z. Liang, and X. Sun, "Microwave Chemistry, Recent Advancements and Eco-Friendly Microwave-Assisted Synthesis of Nanoarchitectures and Their Applications: A Review," *Mater. Today Nano*, vol. 2, no. 13, p. 100076, Apr. 2020.

[49] T. Rajkumar, D. Kukkar, K. H. Kim, J. R. Sohn, and A. Deep, "Cyclodextrin-metal–organic framework (CD-MOF): From synthesis to applications," *Journal of Industrial and Engineering Chemistry*, vol. 72. Korean Society of Industrial

Engineering Chemistry, pp. 50–66, 25-Apr-2019.

[50] L. Zhang *et al.*, "NH $_2$ -MIL-53(Al) Metal–Organic Framework as the Smart Platform for Simultaneous High-Performance Detection and Removal of Hg $^{2+}$," *Inorg. Chem.*, vol. 58, no. 19, pp. 12573–12581, Oct. 2019.

[51] B. H. Liu, D. X. Liu, K. Q. Yang, S. J. Dong, W. Li, and Y. J. Wang, "A new cluster-based metal-organic framework with triazine backbones for selective luminescent detection of mercury(II) ion," *Inorg. Chem. Commun.*, vol. 90, pp. 61–64, Apr. 2018.

[52] A. Stratton, M. Ericksen, T. V. Harris, N. Symmonds, and T. P. Silverstein, "Mercury(II) binds to both of chymotrypsin's histidines, causing inhibition followed by irreversible denaturation/aggregation," *Protein Sci.*, vol. 26, no. 2, pp. 292–305, Feb. 2017.

[53] Y. Zhao, D. Wang, W. Wei, L. Cui, C. W. Cho, and G. Wu, "Effective adsorption of mercury by Zr(IV)-based metal-organic frameworks of UiO-66-NH2 from aqueous solution," *Environ. Sci. Pollut. Res.*, pp. 1–8, Oct. 2020.

[54] X. Zhang, T. Xia, K. Jiang, Y. Cui, Y. Yang, and G. Qian, "Highly sensitive and selective detection of mercury (II) based on a zirconium metal-organic framework in aqueous media," *J. Solid State Chem.*, vol. 253, pp. 277–281, Sep. 2017.

[55] T. Xia *et al.*, "A Terbium Metal–Organic Framework for Highly Selective and Sensitive Luminescence Sensing of Hg2+Ions in Aqueous Solution," *Chem. - A Eur. J.*, vol. 22, no. 51, pp. 18429–18434, 2016.

[56] Y.-Q. Su, Y.-H. Qu, L. Fu, and G.-H. Cui, "An unprecedented binodal (4,6)-connected Co(II) MOF as dual-responsive luminescent sensor for detection of acetylacetone and Hg2+ ions," *Inorg. Chem. Commun.*, vol. 118, p. 108013, Jun. 2020.

[57] D. T. Sun *et al.*, "Rapid, Selective Heavy Metal Removal from Water by a Metal-Organic Framework/Polydopamine Composite," *ACS Cent. Sci.*, vol. 4, no. 3, pp. 349–356, Mar. 2018.

[58] D. Xie *et al.*, "Bifunctional NH2-MIL-88(Fe) metal-organic framework nanooctahedra for highly sensitive detection and efficient removal of arsenate in aqueous media," *J. Mater. Chem. A*, vol. 5, no. 45, pp. 23794–23804, Nov. 2017.

[59] B. K. Gale, M. A. Eddings, S. O. Sundberg, A. Hatch, J. Kim, and T. Ho, "Low-Cost MEMS Technologies," in *Comprehensive Microsystems*, vol. 1. pp. 341–378.

[60] J. Wang *et al.*, "Gas Detection Microsystem with MEMS Gas Sensor and Integrated Circuit," *IEEE Sens. J.*, vol. 18, no. 16, pp. 6765–6773, Aug. 2018.

[61] R. Prajesha, N. Jaina, V. K. Khannaa, V. Guptac, and A. Agarwala, "MEMS based Integrated Gas Sensor for NO2 and NH3," 2015.

[62] A. Bouchaala *et al.*, "Nonlinear-based MEMS sensors and active switches for gas detection," *Sensors (Switzerland)*, vol. 16, no. 6, 2016.

[63]   N. Jaber, S. Ilyas, O. Shekhah, M. Eddaoudi, and M. I. Younis, "Resonant Gas Sensor and Switch Operating in Air with Metal-Organic Frameworks Coating," *J. Microelectromechanical Syst.*, vol. 27, no. 2, pp. 156–163, Apr. 2018.

[64]   B. Chocarro-Ruiz *et al.*, "A CO2 optical sensor based on self-assembled metal-organic framework nanoparticles," *J. Mater. Chem. A*, vol. 6, no. 27, pp. 13171–13177, 2018.

[65]   S. Sachdeva *et al.*, "Gas Phase Sensing of Alcohols by Metal Organic Framework-Polymer Composite Materials," *ACS Appl. Mater. Interfaces*, vol. 9, no. 29, pp. 24926–24935, 2017.

[66]   Sineo, "MDS-6G Digestion Microwave," 2019. [Online]. Available: http://www.sineomicrowave.com/pro.aspx. [Accessed: 15-Nov-2019].

[67]   Horiba LTD, "PTI QuantaMaster 300 Phosphorescene/Fluoroscence Spectrometer." [Online]. Available: https://www.horiba.com/fileadmin/uploads/Scientific/Fluorescence/Downloads/QM-300.pdf. [Accessed: 13-Nov-2019].

[68]   Horiba LTD, "FelixGX Software User's Manual." [Online]. Available: https://bif.wisc.edu/wp-content/uploads/sites/389/2017/11/FelixGX_Ver_4.0.1_Users_Manual.pdf. [Accessed: 13-Nov-2019].

[69]   "Model FD 23," 2020. [Online]. Available: https://www.binder-world.com/en/products/drying-and-heating-chambers/series-fd-classicline/fd-23. [Accessed: 07-Nov-2020].

[70]   "Fourier Transform Infrared Spectroscopy (FTIR) | PerkinElmer," 2020. [Online]. Available: https://www.perkinelmer.com/category/infrared-spectroscopy-ft-ir. [Accessed: 07-Nov-2020].

[71]   Bruker, "The D8 advance family,." [Online]. Available: https://www.bruker.com/products/x-ray-diffraction-and-elemental-analysis/x-ray-diffraction/d8-advance.html. [Accessed: 13-Nov-2019].

[72]   Tescan, "VEGA3." [Online]. Available: https://www.tescan.com/en-us/technology/sem/vega3. [Accessed: 13-Nov-2019].

[73]   Apreo, "Apreo 2 SEM." [Online]. Available: https://www.thermofisher.com/order/catalog/product/APREOSEM. [Accessed: 13-Nov-2019].

[74]   Shimadzu, "Measurement Methods for Powder Samples." [Online]. Available: https://www.shimadzu.com/an/ftir/support/ftirtalk/talk8/intro.html. [Accessed: 13-Nov-2019].

[75]   P. Wu *et al.*, "Cadmium-Based Metal-Organic Framework as a Highly Selective and Sensitive Ratiometric Luminescent Sensor for Mercury(II)," *Inorg. Chem.*, vol. 54, no. 23, pp. 11046–11048, Nov. 2015.

[76]   A. Cetin, O. Esenturk, and E. N. Esenturk, "Optical and Vibrational Properties of [Pt@Pb12]2–, [Ni@Pb12]2–, and [Ni@Pb10]2– Zintl Ion Clusters," *Eur. J. Inorg. Chem.*, vol. 2017, no. 18, pp. 2413–2421, May 2017.

[77] M. Baker, E. Gazi, M. Brown, J. Shanks, P. Gardner, and N. Clarke, "FTIR-based spectroscopic analysis in the identification of clinically aggressive prostate cancer," *Br. J. Cancer*, vol. 99, no. 11, pp. 1859–1866, 2008.

[78] G. Li, F. Li, J. Liu, and C. Fan, "Fe-based MOFs for photocatalytic N2 reduction: Key role of transition metal iron in nitrogen activation," *J. Solid State Chem.*, vol. 285, p. 121245, May 2020.

[79] N. Torres *et al.*, "Implications of structual differences between Cu-BTC and Fe-BTC on their hydrogen storage capactiy," *Colloids surfaces a physiochem*, vol. 5, no. 19, pp. 138–146, 2008.

[80] R. Liang, F. Jing, L. Shen, N. Qin, and L. Wu, "MIL-53(Fe) as a highly efficient bifunctional photocatalyst for the simultaneous reduction of Cr(VI) and oxidation of dyes," *J. Hazard. Mater.*, vol. 287, pp. 364–372, Apr. 2015.

[81] P. Wu *et al.*, "Cadmium-Based Metal–Organic Framework as a Highly Selective and Sensitive Ratiometric Luminescent Sensor for Mercury(II)," *Inorg. Chem.*, vol. 54, no. 23, pp. 11046–11048, Dec. 2015.

[82] J. Carlos Rendón-Balboa *et al.*, "Structure of a luminescent 3D coordination polymer constructed with a trinuclear core of cadmium-trimesate and isoquinoline," *Inorganica Chim. Acta*, vol. 483, pp. 235–240, Nov. 2018.

[83] Z. Liang, C. Qu, W. Guo, R. Zou, and Q. Xu, "Pristine Metal–Organic Frameworks and their Composites for Energy Storage and Conversion," *Advanced Materials*, vol. 30, no. 37. 13-Sep-2018.

[84] M. Jouyandeh, F. Tikhani, S. Moghari, V. Akbari, and X. Gabrion, "Synthesis, characterization, and high potential of 3D metal–organic framework (MOF) nanoparticles for curing with epoxy," *J. Alloys Compd.*, vol. 829, p. 154547, Jul. 2020.

[85] C. B. Liu, X. J. Zheng, Y. Y. Yang, and L. P. Jin, "Template-assisted assembly of porous lanthanide coordination polymers with 2-aminoterephthalic acid," *Inorg. Chem. Commun.*, vol. 8, no. 11, pp. 1045–1048, Nov. 2005.

[86] J. Arias-Pardilla, H. J. Salavagione, C. Barbero, E. Morallón, and J. L. Vázquez, "Study of the chemical copolymerization of 2-aminoterephthalic acid and aniline. Synthesis and copolymer properties," *Eur. Polym. J.*, vol. 42, no. 7, pp. 1521–1532, Jul. 2006.

[87] X. Y. Chen, V. T. Hoang, D. Rodrigue, and S. Kaliaguine, "Optimization of continuous phase in amino-functionalized metal-organic framework (MIL-53) based co-polyimide mixed matrix membranes for CO 2/CH4 separation," *RSC Adv.*, vol. 3, no. 46, pp. 24266–24279, 2013.

[88] G. Derkachov, D. Jakubczyk, K. Kolwas, K. Piekarski, Y. Shopa, and M. Woźniak, "Dynamic light scattering investigation of single levitated micrometre-sized droplets containing spherical nanoparticles," *Meas. J. Int. Meas. Confed.*, vol. 158, p. 107681, Jul. 2020.

[89] S. E. Miller, M. H. Teplensky, P. Z. Moghadam, and D. Fairen-Jimenez, "Metal-organic frameworks as biosensors for luminescence-based detection and

imaging," *Interface Focus*, vol. 6, no. 4. 06-Aug-2016.

[90] R. Giovine, C. Volkringer, J. Trébosc, J. P. Amoureux, and T. Loiseau, "NMR crystallography to probe the breathing effect of the MIL-53(Al) metal-organic framework using solid-state NMR measurements of 13C-27Al distances," in *Acta Crystallographica Section C: Structural Chemistry*, 2017, vol. 73, no. 3, pp. 176–183.

[91] A. Pankajakshan, D. Kuznetsov, and S. Mandal, "Ultrasensitive Detection of Hg(II) Ions in Aqueous Medium Using Zinc-Based Metal-Organic Framework," *Inorg. Chem.*, vol. 58, no. 2, pp. 1377–1381, Jan. 2019.

[92] N. D. Rudd *et al.*, "Highly Efficient Luminescent Metal-Organic Framework for the Simultaneous Detection and Removal of Heavy Metals from Water," *ACS Appl. Mater. Interfaces*, vol. 8, no. 44, pp. 30294–30303, Nov. 2016.

[93] Y. J. Yang, D. Liu, Y. H. Li, and G. Y. Dong, "Two new luminescent ternary Cd(II)-MOFs by regulation of aromatic dicarboxylate ligands used as efficient dual-responsive sensors for toxic metal ions in water," *Polyhedron*, vol. 159, pp. 32–42, Feb. 2019.

[94] P. Naula, A. Airola, S. Pihlasalo, I. Montoya Perez, T. Salakoski, and T. Pahikkala, "Assessment of metal ion concentration in water with structured feature selection," *Chemosphere*, vol. 185, pp. 1063–1071, Oct. 2017.

[95] S. Paul, A. Mandal, P. Bhattacharjee, S. Chakraborty, R. Paul, and B. Kumar Mukhopadhyay, "Evaluation of water quality and toxicity after exposure of lead nitrate in fresh water fish, major source of water pollution," *Egypt. J. Aquat. Res.*, vol. 45, no. 4, pp. 345–351, Dec. 2019.

[96] M. I. N. Ahamed, S. Rajeshkumar, V. Ragul, S. Anand, and K. Kaviyarasu, "Chromium remediation and toxicity assessment of nano zerovalent iron against contaminated lake water sample (Puliyanthangal Lake, Tamilnadu, India)," *South African J. Chem. Eng.*, vol. 25, pp. 128–132, Jun. 2018.

[97] S. A. A. Razavi, M. Y. Masoomi, and A. Morsali, "Double Solvent Sensing Method for Improving Sensitivity and Accuracy of Hg(II) Detection Based on Different Signal Transduction of a Tetrazine-Functionalized Pillared Metal-Organic Framework," *Inorg. Chem.*, vol. 56, no. 16, pp. 9646–9652, Aug. 2017.

[98] S. Jayabal, R. Sathiyamurthi, and R. Ramaraj, "Selective sensing of Hg2+ ions by optical and colorimetric methods using gold nanorods embedded in a functionalized silicate sol-gel matrix," *J. Mater. Chem. A*, vol. 2, no. 23, pp. 8918–8925, Jun. 2014.

[99] V. Kumar, P. K. Bharti, M. Talwar, A. K. Tyagi, and P. Kumar, "Studies on high iron content in water resources of Moradabad district (UP), India," *Water Sci.*, vol. 31, no. 1, pp. 44–51, Apr. 2017.

[100] Y. Guan, M. Xia, X. Wang, W. Cao, and A. Marchetti, "Water-based preparation of nano-sized NH2-MIL-53(Al) frameworks for enhanced dye removal," *Inorganica Chim. Acta*, vol. 484, pp. 180–184, 2019.

[101] K. Wang, J. Gu, and N. Yin, "Efficient Removal of Pb(II) and Cd(II) Using NH

2-Functionalized Zr-MOFs via Rapid Microwave-Promoted Synthesis," *Ind. Eng. Chem. Res.*, vol. 5, no. 15, pp. 22–41, 2017.

[102] Z. Seyfi Hasankola, R. Rahimi, H. Shayegan, E. Moradi, and V. Safarifard, "Removal of Hg2+ heavy metal ion using a highly stable mesoporous porphyrinic zirconium metal-organic framework," *Inorganica Chim. Acta*, vol. 501, p. 119264, Feb. 2020.

[103] B. Seoane, C. Téllez, J. Coronas, and C. Staudt, "NH2-MIL-53(Al) and NH2-MIL-101(Al) in sulfur-containing copolyimide mixed matrix membranes for gas separation," *Sep. Purif. Technol.*, vol. 111, pp. 72–81, Jun. 2013.

[104] Y. Fu *et al.*, "Temperature modulation of defects in NH2-UiO-66(Zr) for photocatalytic CO2 reduction," *RSC Adv.*, vol. 9, no. 65, pp. 37733–37738, Nov. 2019.

[105] M. Ma, A. Bétard, I. Weber, N. S. Al-Hokbany, R. A. Fischer, and N. Metzler-Nolte, "Iron-based metal-organic frameworks MIL-88B and NH2-MIL-88B: High quality microwave synthesis and solvent-induced lattice 'breathing,'" *Cryst. Growth Des.*, vol. 13, no. 6, pp. 2286–2291, Jun. 2013.

[106] S. N. Kim *et al.*, "Metal-organic frameworks, NH2-MIL-88(Fe), as carriers for ophthalmic delivery of brimonidine," *Acta Biomater.*, vol. 79, pp. 344–353, Oct. 2018.

[107] A. Pankajakshan, D. Kuznetsov, and S. Mandal, "Ultrasensitive Detection of Hg(II) Ions in Aqueous Medium Using Zinc-Based Metal-Organic Framework," *Inorg. Chem.*, vol. 58, no. 2, pp. 1377–1381, Jan. 2019.

Heat maps for the NH$_2$-Cd-BDC MOF:

Heat maps were performed for the single ion detection and competition tests. The heat maps can be seen in Figure 33, Figure 34 and Figure 35. Figure 33 represent the heat map for the single ion test. Figure 34 represent the heat map for the competition test before the mercury addition. Figure 35 represent the heat map for the competition test after the mercury addition. The color coding scheme is given below:

- Red cells: Indicate a value of p less than or equal to 0.001
- Orange color: Indicate a value of p less than or equal to 0.01
- Yellow color: Indicate a value of p less than 0.05
- Grey color: Indicate a value of p equal to or greater than 0.05

	Mercury	Iron	Calcium	Sodium	Potassium	Cadmium	Copper	Chromium	Lead
Mercury	1	7.36251E-08	1.48126E-13	1.48126E-13	1.48126E-13	1.48126E-13	5.94031E-06	6.69957E-07	2.60047E-10
Iron	7.36251E-08	1	8.17179E-09	8.17179E-09	8.17179E-09	8.17179E-09	4.39747E-06	0.000125887	4.77946E-08
Calcium	1.48126E-13	8.17179E-09	1	0	0	0	6.69133E-09	8.70861E-07	1.39493E-07
Sodium	1.48126E-13	8.17179E-09	0	1	0	0	6.69133E-09	8.70861E-07	1.39493E-07
Potassium	1.48126E-13	8.17179E-09	0	0	1	0	6.69133E-09	8.70861E-07	1.39493E-07
Cadmium	1.48126E-13	8.17179E-09	0	0	0	1	6.69133E-09	8.70861E-07	1.39493E-07
Copper	5.94031E-06	4.39747E-06	6.69133E-09	6.69133E-09	6.69133E-09	6.69133E-09	1	4.45482E-06	2.29618E-08
Chromium	6.69957E-07	0.000125887	8.70861E-07	8.70861E-07	8.70861E-07	8.70861E-07	4.45482E-06	1	5.37276E-06
Lead	2.60047E-10	4.77946E-08	1.39493E-07	1.39493E-07	1.39493E-07	1.39493E-07	2.29618E-08	5.37276E-06	1

Figure 33: Heat map for single ion test.

	Iron	Copper	Cadmium	Sodium	Potassium	Calcium	Lead	Chromium
Iron	1	0.018402487	1.27922E-11	1.27922E-11	1.27922E-11	1.27922E-11	6.7896E-08	1.31E-05
Copper	0.018402487	1	4.08747E-10	4.08747E-10	4.08747E-10	4.08747E-10	1.37273E-07	1.87E-05
Cadmium	1.27922E-11	4.08747E-10	1	0	0	0	1.72217E-08	1.17E-07
Sodium	1.27922E-11	4.08747E-10	0	1	0	0	1.72217E-08	1.17E-07
Potassium	1.27922E-11	4.08747E-10	0	0	1	0	1.72217E-08	1.17E-07
Calcium	1.27922E-11	4.08747E-10	0	0	0	1	1.72217E-08	1.17E-07
Lead	6.7896E-08	1.37273E-07	1.72217E-08	1.72217E-08	1.72217E-08	1.72217E-08	1	4.59E-05
Chromium	1.30837E-05	1.8703E-05	1.16727E-07	1.16727E-07	1.16727E-07	1.16727E-07	4.59137E-05	1

Figure 34: Heat map for competition test before mercury addition.

	Iron	Copper	Cadmium	Sodium	Potassium	Calcium	Lead	Chromium
Iron	1	0.81235423	0.002724493	3.08918E-08	1.57139E-08	1.44196E-05	0.026877842	1.69E-05
Copper	0.81235423	1	0.002053599	1.26399E-08	3.78397E-09	1.40113E-05	0.006190892	3.45E-06
Cadmium	0.002724493	0.002053599	1	1.10269E-07	7.47746E-08	2.16092E-05	0.000461656	1.34E-05
Sodium	3.08918E-08	1.26399E-08	1.10269E-07	1	0.689119362	0.205354342	4.01828E-09	1.84E-09
Potassium	1.57139E-08	3.78397E-09	7.47746E-08	0.689119362	1	0.217542587	2.21754E-10	3.1E-11
Calcium	1.44196E-05	1.40113E-05	2.16092E-05	0.205354342	0.217542587	1	1.22009E-05	6.98E-06
Lead	0.026877842	0.006190892	0.000461656	4.01828E-09	2.21754E-10	1.22009E-05	1	1.93E-07
Chromium	1.69489E-05	3.4489E-06	1.34231E-05	1.83561E-09	3.10322E-11	6.97598E-06	1.92943E-07	1

Figure 35: Heat map for competition test after mercury addition.

Vita

Bassam El Taher was born in 1995, in Sharjah, United Arab Emirates. He received his primary and secondary education in Dubai, UAE. He received his B.Sc. degree in Chemical Engineering from the American University of Sharjah in 2018. From 2018 to 2019, he worked as a Project Engineer in Crescent Petroleum.

In January 2019, he joined the Biomedical Engineering master's program in the American University of Sharjah as a graduate research assistant. During his master's study, he co-authored 1 paper which was published in the journal of Colloids and Surfaces A: Physiochemical and Engineering Aspects. His research interests are in water treatment and process engineering.